Reciprocal cybrids reveal how organellar genomes affect plant phenotypes

Pádraic J Flood, Tom P J M Theeuwen, Korbinian Schneeberger, Paul Keizer, Willem Kruijer, Edouard Severing, Evangelos Kouklas, Jos A Hageman, Raúl Wijfjes, Vanesa Calvo-Baltanas, et al.

Title: Reciprocal cybrids reveal how organellar genomes affect plant phenotypes

Authors:

Pádraic J. Flood[1,2,3†*], Tom P.J.M. Theeuwen[1†*], Korbinian Schneeberger[3], Paul Keizer[4], Willem Kruijer[4], Edouard Severing[3], Evangelos Kouklas[1], Jos A. Hageman[4], Raúl Wijfjes[5], Vanesa Calvo-Baltanas[1], Frank F.M. Becker[1], Sabine K. Schnabel[4], Leo A.J. Willems[6], Wilco Ligterink[6], Jeroen van Arkel[7], Roland Mumm[7], José M. Gualberto[8], Linda Savage[9], David M. Kramer[9], Joost J.B. Keurentjes[1], Fred van Eeuwijk[4], Maarten Koornneef[1,3], Jeremy Harbinson[2], Mark G.M. Aarts[1] & Erik Wijnker[1*]

Affiliations:

[1] Laboratory of Genetics, Wageningen University & Research, Wageningen, The Netherlands.

[2] Horticulture and Product Physiology, Wageningen University & Research, Wageningen, The Netherlands.

[3] Department of Plant Developmental Biology, Max Planck Institute for Plant Breeding Research, Cologne, Germany.

[4] Biometris, Wageningen University & Research, Wageningen, The Netherlands.

[5] Bioinformatics Group, Wageningen, The Netherlands

[6] Laboratory of Plant Physiology, Wageningen University & Research, Wageningen, The Netherlands.

[7] Bioscience, Wageningen University & Research, Wageningen, The Netherlands

[8] Institut de Biologie Moléculaire des Plantes, CNRS, Université de Strasbourg, Strasbourg, France.

[9] MSU-DOE Plant Research Lab, Michigan State University, East Lansing, USA

[†] These authors contributed equally to this work

* Correspondence to:

P.J. Flood - flood@mpipz.mpg.de

T.P.J.M. Theeuwen - tom.theeuwen@wur.nl

E. Wijnker - erik.wijnker@wur.nl

Introductory paragraph:

Assessing the impact of variation in chloroplast and mitochondrial DNA (collectively termed the plasmotype) on plant phenotypes is challenging due to the difficulty in separating their effect from nuclear derived variation (the nucleotype). Haploid inducer lines can be used as efficient plasmotype donors to generate new plasmotype-nucleotype combinations (cybrids)[1]. We generated a panel comprising all possible cybrids of seven *Arabidopsis thaliana* accessions and extensively phenotyped these lines for 1859 phenotypes under stable and fluctuating conditions. We show that natural variation in the plasmotype results in additive as well as epistatic effects across all phenotypic categories. Plasmotypes which induce more additive phenotypic changes also cause more significant epistatic effects, suggesting a possible common basis for both additive and epistatic effects. On average epistatic interactions explained twice as much of the variance in phenotypes as additive plasmotype effects. The impact of plasmotypic variation was also more pronounced under fluctuating and stressful environmental conditions. Thus, the phenotypic impact of variation in plasmotypes is the outcome of multilevel Nucleotype x Plasmotype x Environment interactions and, as such, the plasmotype is likely to serve as a reservoir of variation which is predominantly exposed under certain conditions. The production of cybrids using haploid inducers is a quick and precise method for assessing the phenotypic effects of natural variation in organellar genomes. It will facilitate efficient screening of unique nucleotype-plasmotype combinations to both improve our understanding of natural variation in nucleotype-plasmotype interactions and identify favourable combinations to improve plant performance.

Chloroplasts and mitochondria play essential roles in metabolism, cellular homeostasis and environmental sensing [2,3]. Their genomes contain only a limited set of genes whose functioning requires tight coordination with the nucleus through signaling pathways that modulate nuclear and organellar gene expression [3,4]. Plasmotype variation can be strongly additive, such as in the case of chloroplast encoded herbicide tolerance [5], or can manifest itself in complex cytonuclear interactions as non-additive, non-linear effects (epistasis), such as found for secondary metabolites [6]. The phenotypic consequences of epistasis can be detected when a plasmotype causes phenotypic effects in combination with some, but not all, nuclear backgrounds. Recent studies suggest that cytonuclear epistasis is the main route through which variation in the plasmotype is expressed [6-12] and that additive effects are both rare and of small effect.

Plasmotypic variation is relevant from an agricultural as well as evolutionary perspective [13-15], but to understand or utilize it, it is necessary to separate nuclear from mitochondrial and chloroplastic effects. Reciprocal-cross designs, where nucleotypes segregate in different plasmotypic backgrounds, have been used to identify plasmotype-specific quantitative trait loci [6,10], but are limited to just two plasmotypes. A larger number of plasmotypes can be studied using backcross designs where plasmotypes are introgressed into different nuclear backgrounds [11,16-18], but backcross approaches are lengthy and any undetected nuclear introgressions may confound the results.

To precisely and rapidly address the contribution of organellar variation to plant phenotypes, we explored the use of a haploid inducer line available in *Arabidopsis* (*GFP-tailswap*) [1,19]. When pollinated with a wild-type plant, the *GFP-tailswap* nuclear genome is lost from the zygote through uniparental genome elimination. This generates haploid cybrid offspring with a paternally derived nuclear genome and maternally (*GFP-tailswap*) derived mitochondria and chloroplasts (Fig. 1). These haploid plants produce stable diploid (doubled haploid) offspring following genome duplication or restitutional meiosis [19]. We set out to test the use of this approach to investigate how plasmotypic variation affects plant phenotypes and to what extent this variation manifests itself as additive variation or as cytonuclear epistasis.

Seven different *Arabidopsis* accessions were selected for our experiment: six that represent a snapshot of natural variation (Bur, C24, Col-0, L*er*-0. Sha, WS-4) and Ely, an accession with a large-effect mutation in the chloroplast-encoded *PsbA* gene [20]. This mutation results in reduced photosystem II efficiency [20,21] and was included to evaluate the consequence of a strong plasmotype effect in our test-panel. We first generated haploid inducers for all seven plasmotypes (Fig. 1a) and then used each inducer to generate cybrid offspring for all seven nucleotypes (Figs. 1b and c). Cybrid genotypes will henceforth be denoted as nucleotype^{plasmotype} (i.e. Ely^{Bur} denotes a cybrid with Ely nucleotype and Bur plasmotype). Wild-type nucleotype-plasmotype combinations were also regenerated in this way (hereafter referred to as self-cybrids; i.e. Bur^{Bur}, C24^{C24}, etc.) to later compare these with their wild-type progenitors. The genotypes of all haploid cybrids were verified by whole genome resequencing. This led to the exclusion of Bur^{C24} and Bur^{Bur}, which were identified to contain the exact same nucleotypic *de-novo* duplication of 200 kb, likely derived from a spontaneous duplication in a Bur wild-type progenitor used in creating these cybrids (see Online methods; Extended Data Fig. 1). With the exception of Ely^{Sha} for which we obtained seeds at a later stage, we obtained

doubled haploid seeds from all haploid cybrids resulting in a test panel of 46 cybrids and 7 wild-type progenitors. As with Ely^{Sha}, Bur^{C24} and Bur^{Bur} were subsequently recreated, and the complete panel will be submitted to the European Arabidopsis Stock Centre (www.arabidopsis.info). To visualize the genetic variation between lines within our panel we generated neighbor joining trees for the nuclear, mitochondrial and chloroplast genomes (Extended Data Fig. 2; Supplementary Figs. 1 to 3). The nucleotypes were found to be approximately equidistant, while the L*er*, Ely and Col plasmotypes appear to be more closely related to each other than the other plasmotypes.

We phenotyped the cybrid panel under constant environmental conditions for absolute and relative growth rate, biomass accumulation, epinastic leaf movement, photosystem II (PSII) efficiency (Φ_{PSII}), non-photochemical quenching (NPQ) and elements thereof ($\Phi_{NO,}$ Φ_{NPQ}, q_E and q_I), a reflectance-based estimate of chlorophyll, flowering time, germination, pollen abortion, and primary metabolites. To simulate more variable conditions that are frequently encountered in the field, we also screened the panel under fluctuating light for all the above-mentioned photosynthesis-related phenotypes and assayed germination rates under osmotic stress and after a controlled deterioration treatment. Counting individual metabolite concentrations and single time points in the time series separately, we collected in total 1859 phenotypes (Supplementary Data 1, Supplementary Table 4). To avoid overrepresentation of highly correlated and non-informative phenotypes we selected a subset of 92 phenotypes (Online methods, Supplementary Table 2) comprising 24 from constant growth conditions, 32 from fluctuating or challenging environmental conditions and 36 primary metabolites, for further analysis (Extended Data Fig. 3, Supplementary Table 2).

Comparison of six self-cybrids with their genetically identical wild-type progenitors for these 92 phenotypes did not reveal significant phenotypic differences (Supplementary Table 1), from which we infer that uniparental genome elimination is a robust method to generate cybrids. To determine the relative contributions of nucleotype, plasmotype, and their interaction to the observed phenotypic variation, we estimated the fraction of the broad sense heritability (H^2; also called repeatability [22]) explained by each. Across the entire panel the average contribution to H^2 of nucleotype, plasmotype and nucleotype-plasmotype interaction was 65.9%, 28.0% and 6.1% respectively (Supplementary Tables 2 and 3; Supplementary Data 2). Most of the plasmotype-derived additive variation was caused by the Ely plasmotype, arising from the *psbA* mutation. When this plasmotype was excluded from the analysis, the nucleotype, plasmotype and their interaction account for 91.9%, 2.9% and 5.2% of the

genetic variation, respectively (Supplementary Tables 2 and 3; Supplementary Data 2). So, while nucleotype-derived additive variation is the main genetic determinant of the cybrid phenotype, variation caused by plasmotype additive effects as well as epistatic effects results in substantial phenotypic differences.

Next we sought to assess whether there are general patterns in how specific nucleotypes and plasmotypes interact. To this end we first assessed which plasmotype changes result in additive phenotypic changes. Plasmotype replacements involving the Ely plasmotype lead to additive changes in, on average, 50 (out of 92) phenotypes across the 7 nucleotypes (Table 1a). Changes involving the Bur plasmotype lead to on average 10 significant additive effects, 8 of which are photosynthesis-related (Supplementary Data 2). Other plasmotype changes show on average one additive effect, in predominantly non-photosynthetic phenotypes. Comparison of wild-type cytonuclear combinations with all their iso-nuclear cybrid lines also shows that plasmotype changes involving Ely and Bur plasmotypes show the most epistatic effects (on average 43 and 6 respectively) (Table 1b). The number of epistatic effects resulting from the Bur plasmotype range between 0 ($L\mathit{er}^{Ler}$ vs $L\mathit{er}^{Bur}$) to 10 (Sha^{Sha} vs Sha^{Bur}), indicating high variability. Plasmotype changes involving other plasmotypes show more modest numbers of significant epistatic effects that range from 0 to 6. Plasmotypes that result in more additive effects also cause more epistatic effects (Pearson correlation coefficient of 0.99, p-value 1.3e-5) suggesting a possible common cause (Extended Data Fig. 4).

Though the average total explained variance due to the cytonuclear epistasis is only 5.2%, these interactions can have strong effects for specific phenotypes or in specific cybrids. Explained variance for some phenotypes can be markedly higher, for example, for projected leaf area this amounts to 12.3%, for hyponastic leaf movement to 8.3% and for ΦNPQ to 17.8%. A strong epistatic effect in pollen abortion (43.5%) was due to relatively high pollen abortion in Sha^{Sha} (Fig. 2a) which we also observed in the Sha wild type. The higher pollen abortion in its native nucleotype is surprising and could indicate incomplete compensation due to the accumulation of deleterious variants or perhaps to facilitate increased outcrossing. The only cybrid for which we initially failed to obtain seed was Ely^{Sha}. This haploid was recreated and pollinated with wild-type Ely pollen to increase the chance of seed set. The diploid offspring showed 45% of pollen abortion and despite having pollen, all plants were male sterile. This indicates that in combination with the Ely nucleotype the Sha plasmotype results in full cytoplasmic male sterility (Extended Data Fig. 5). In combination with the Sha plasmotype, pollen

abortion across the seven nucleotypes can range from near zero, to 8.9% in the Sha^{Sha} self-cybrid and to full male sterility in Ely^{Sha}, exemplifying the degree to which epistasis can manifest itself.

Cybrids with the Ely plasmotype exhibit strong additive effects: all have a lower PSII efficiency (Φ_{PSII}) (Fig. 2b) and lower values for other photosynthesis-related phenotypes i.e. NPQ, q_E and chlorophyll content (Fig. 2c and Supplementary Data 2). This reduced Φ_{PSII} is likely to be responsible for the concomitant reductions in biomass, growth rate and seed size and altered primary metabolite concentration (Supplementary Data 2). To test whether additive effects could also be detected at the level of gene expression we contrasted the transcriptome of Ely^{Ely} with that of the Ely^{Ler} and Ely^{Bur} cybrids. We also compared the transcriptomes of Ler^{Ler}, Ler^{Bur}, *and* Ler^{Ely} (Supplementary Data 3; for details see Extended Data Fig. 6 and Supplementary Table 5). Exchanging the Ely plasmotype with L*er* or Bur, in either the L*er* or Ely nuclear background, resulted in a consistent change in the expression of 40 genes, of which most were upregulated (Supplementary Table 6). A GO-term analysis revealed that these genes are significantly enriched for those involved in photorespiration (GO:0009853) and in glycine- and serine family amino acid metabolism (GO:0006544 and GO:0009069) (Supplementary Data 3). This is in line with the low serine and glycine content of cybrids with the Ely plasmotype, which suggests reduced photorespiration (Supplementary Data 2) [23] and can be linked to lower overall photosynthetic activity.

The Ely plasmotype was deliberately included in our panel for its strong additive effect. In addition to Ely we also observed strong additive effects from the Bur plasmotype which are mainly restricted to the photosynthetic parameters. Under normal conditions PSII efficiency is already slightly increased by the Bur plasmotype (1.6%), however when fluctuating the light intensity, this difference becomes more apparent (3.5% increase) (Figs. 2b and 3, Extended Data Fig. 7). This increase in Φ_{PSII} under fluctuating conditions results in a corresponding reduction in Φ_{NO} and Φ_{NPQ} of 7.3% and 2.2% respectively. NPQ, q_E and q_I are also influenced by the plasmotype, but the time points at which these differences occur differ per phenotype (Figs. 3a and b). The Bur plasmotype increases NPQ, with the largest increase of 5.9% at the beginning of day 2 (38.46 h) (Fig. 2c), while the rapidly reversible component of NPQ, q_E, has a maximum reduction of 26.6% at the end of day 3 (71.46 h) (Fig. 2d).

These photosynthesis-related phenotypes are likely to be due to chloroplast-derived variation. In support of a chloroplastic origin for this photosynthetic variation, measurements of mitochondrial respiration suggest that Bur is not an outlier and shows standard respiration rates (Extended Data Fig.

8). Based on DNA sequence coverage plots there are no obvious duplications or deletions in the mitochondrial or chloroplast sequence of Bur thus we expect that altered expression or protein activity, as opposed to gene gain or loss, is driving the Bur-derived phenotypes (Extended Data Fig. 9). We annotated the sequence variation of all plasmotypes using SnpEff [24]. From this we found no large-effect mutations in the Bur mitochondria. There were, however, unique missense variants in the chloroplastic genes *MATURASE K* (*MATK*), *NAD(P)H-QUINONE OXIDOREDUCTASE SUBUNIT 6* (*NDHG*) and the chloroplast open reading frame 1 (*YCF1*) as well as a frameshift mutation in tRNA-Lys (*TRNK*) (Supplementary Data 4). Of these, NDHG is noteworthy because of its functions. It is part of the NAD(P)H-dehydrogenase-like complex (NDH) that is located inside the thylakoid membrane and acts, amongst others, as a proton pump in cyclic electron flow around photosystem I and chlororespiration. NDH creates a pH differential that generates non-photochemical quenching (Strand et al., 2017; Laughlin et al., 2019). However, determining as to whether the missense mutation in NDH underlies the observed phenotypic changes in the photosynthetic parameters would require further experimentation. In contrast to Ely, the plasmotype which spread in response to the use of herbicides, an anthropogenic selective pressure [5], the Bur plasmotype represents a naturally occurring plasmotype that has an additive impact on key photosynthetic phenotypes.

Our experiments have shown that a clean, systematic exploration of plasmotypic variation in a plant species is feasible. To our knowledge, apart from the *cenh3* mutant used here, there is only one other intraspecific haploid inducer available (the maize *ig* mutant) which can be used via the maternal line and thus replace the plasmotype [25-27]. Current knowledge of *cenh3* mediated uniparental genome elimination should allow for the creation of maternal haploid inducers in a wider range of species [28]. This would allow elite nucleotypes to be brought into new plasmotypic backgrounds to explore novel plasmotype-nucleotype combinations. Our data indicate that there is substantial variation for phenotypes such as NPQ and Φ_{PSII} which are important for plant productivity [29-31]. Next to Ely we identified one new plasmotype (Bur) that significantly impacts photosynthesis in an additive manner. Expanding our panel would likely find more, suggesting that future research aiming to enhance crop photosynthesis should play close attention to plasmotypic variation. Apart from studying natural variation, the use of haploid inducers as plasmotype donors could be used to transfer cytoplasmic male sterility (CMS), herbicide resistances or genetically engineered plasmotypes. Plant plasmotypes, are notoriously difficult to genetically modify, although recently there have been some advances in this

regard [32-35]. The use of haploid inducers as plasmotype donors could further increase the accessibility of such modifications, as transformations could be undertaken in a compatible nucleotype and once achieved can be transferred into different nucleotypes, thus amplifying the potential impact of successful plasmotype modifications.

Exploring the potential of plasmotypic variation via the use of haploid inducer lines is not only promising for plant breeding, but also for understanding the role such variation plays in plant adaptation [13,14]. Our results show that despite considerable genetic divergence between the genotypes used in our panel, all cybrids were viable, this in itself suggests a remarkable degree of conservation for the fundamental components of cytonuclear interactions. Although we do find clear additive effects of some plasmotypes, the majority of the plasmotype-derived variation manifests as epistasis in the traits we measured which is in line with previous research in plants, animals, and fungi [6-8,11,18]. Also in line with studies of mitonuclear interactions in animals is the observation that phenotypic variation due to plasmotypic variation becomes more pronounced under fluctuating and stressful conditions [18,36-38]. Both our results and previous work suggest that multilevel interactions (i.e. Nucleotype x Plasmotype x Environment) may be the primary mechanism by which plasmotypic variation is expressed. Thus, plasmotypic variation may act as an evolutionary capacitor providing novel phenotypes in specific genetic and environmental contexts. In our rapidly changing climate such variation may be particularly important for both crops and wild species. To fully understand the impact and functional relevance of plasmotypic variation future studies should both expand the number of plasmotypes and the range of environmental conditions assayed. The speed and precision with which new cybrids can be created makes such research feasible.

Online methods

Plant materials: Seven *Arabidopsis* accessions were chosen for the construction of a full nucleotype-plasmotype diallel. Ely (CS28631) is atrazine resistant due to a chloroplast-encoded mutation in *PsbA* which leads to a modified D2 protein that greatly reduces PSII efficiency [20]. Ws-4 (CS5390) was included for its unusual PSII phosphorylation dynamics [39]. Bur (CS76105) is commonly used in diversity panels and is a standard reference accession. Sha (CS76227) was selected based on its capacity to induce cytoplasmic male sterility in some crosses [40]. The set was completed by adding L*er* (CS76164), Col (CS76113) and C24 (CS76106) which are three widely used genotypes in *Arabidopsis* research. Col is the reference for nuclear, mitochondrial, and chloroplast sequences, although at the start of this project C24 was the reference for the mitochondrial sequence, hence its inclusion. The *GFP-tailswap* haploid-inducer that expresses a GFP-tagged CENTROMERE HISTONE 3 protein in a *cenh3/htr12* mutant background, is in a Col background (Ravi and Chan, 2010).

Generation of a nucleotype-plasmotype diallel: To generate new nucleotype-plasmotype combinations, plants of all seven accessions (Bur, C24, Col, Ely, L*er*, Sha and Ws-4) were crossed as males to *GFP-tailswap* resulting in all cybrids with the Col plasmotype. New HI lines were created by crossing the original *GFP-tailswap* line as a male to the six additional plasmotype mothers (Bur, C24, Ely, L*er*, Sha and Ws-4). Genome elimination does not always occur and some of the offspring were diploid F1 lines. These were selfed and F2 lines homozygous for the *cenh3/htr12* mutation and carrying the *GFP-tailswap* were selected as new HI lines in different plasmotypic backgrounds (Fig. 1a). Plants of all seven accessions were then crossed as males to these new HI lines and the haploids arising from these 49 crosses were identified based on their phenotype (as described in Wijnker, et al. [41]). These haploid lines self-fertilized, either following somatic genome duplication or after restitutional meiosis [19], and gave rise to doubled haploid offspring (Fig. 1b). The resulting 49 lines comprise a full diallel of 21 pairs of reciprocal nucleotype-plasmotype combinations (cybrids) as well as seven nucleotype-plasmotype combinations that have, in principle, the same nucleotype-plasmotype combinations as their wild-type progenitors (self-cybrids; Fig. 1c, diagonal). All cybrids and the wild-type accessions were propagated for one generation before use in further experiments, with the exception of Ely^{Sha} of which the original haploid died without setting seed and was recreated at a later stage by generating haploids that were pollinated with Ely wild-type plants to ensure seed set.

Genotype confirmation: To confirm that all cybrids in our panel are authentic, all 49 cybrids and 7 wild-type progenitors were whole-genome sequenced at the Max Planck Genome Centre Cologne (Germany) using Illumina Hiseq 2500 150-bp paired-end sequencing. The cybrids were sequenced at 8.5X coverage and the wild-type progenitors at 40X coverage. To remove erroneous bases, we performed adapter and quality trimming using Cutadapt (version 1.18) [42]. Sequences were clipped if they matched at least 90% of the total length of one of the adapter sequences provided in the NEBNext Multiplex Oligos for Illumina® (Index Primers Set 1) instruction manual. In addition, we trimmed bases from the 5' and 3' ends of reads if they had a phred score of 20 or lower. Reads that were shorter than 70 bp after trimming were discarded. Trimmed reads were aligned to a modified version of the A. thaliana Col-0 reference genome (TAIR10, European Nucleotide Accession number: GCA_000001735.2) which contains an improved assembly of the mitochondrial sequence (Genbank accession number: BK010421) [43] using bwa mem (version 0.7.10-r789) [44] with default parameters. The resulting alignment files were sorted and indexed using samtools (version 1.3.1) [45]. Duplicate read pairs were marked using the MarkDuplicates tool of the GATK suite (version 4.0.2.1), using an optical duplicate pixel distance of 100, as recommended in the documentation of GATK when working with data from unpatterned Illumina flowcells. Variants were called using a workflow based on GATK Best Practices. Base quality scores of aligned reads were recalibrated using GATK BaseRecalibrator with default parameters, using a set of variants of a world-wide panel of 1135 *Arabidopsis* accessions [46] (obtained from ftp://ftp.ensemblgenomes.org/pub/plants/release-37/vcf/arabidopsis_thaliana/) as known sites. Following base recalibration, variants were called in each sample using GATK HaplotypeCaller, allowing for a maximum of three alternate alleles at each site. Samples were then jointly genotyped using GATK GenomicsDBImport and GATK GenotypeGVCFs with default parameters. This last step generated three different VCF files: one containing the calls of the nuclear genome, one containing calls of the mitochondrial genome and one containing calls of the chloroplast genome.

To remove likely false positive calls, we filtered the call sets using two complementary approaches. First, we filtered the nuclear call set using GATK VariantRecalibrator and GATK ApplyVQSR (--truth-sensitivity-filter-level set at 99.9), using the set of variants called in the world-wide panel of 1135 *Arabidopsis* accessions as a training and truth set (prior=10.0). This step could not be

293 performed for the mitochondrial and chloroplast calls, as these lack a golden truth set that can be used
294 for recalibration. Second, we filtered variants based on their quality by depth score (QD). For the
295 nuclear call set, we used a QD score of 40, leaving 3.7 million SNPs, for the chloroplast call set a QD
296 of 25, leaving 356 SNPs and for the mitochondrial call set a QD of 20, leaving 135 SNPs.

297 46 cybrids were found to have the correct genotypes. With one line, $Bur^{Ws\text{-}4}$, there was a
298 sample mix-up during library preparation with Sha^{Sha}, leading to two sequenced Sha^{Sha} samples and
299 no sequenced $Bur^{Ws\text{-}4}$ sample. Fortunately, we did have a true $Bur^{Ws\text{-}4}$ cybrid, which we confirmed
300 based on phenotype (Bur and Sha nucleotypes are phenotypically distinct from one another) and on
301 genotype, using KASP™ markers (see below) (Supplementary Table 8). Two other lines, $C24^{C24}$ and
302 $Ws\text{-}4^{Col}$, had a high number of heterozygous calls in their plasmotypes, with $C24^{C24}$ being
303 heterozygous with $C24^{Col}$ and $Ws\text{-}4^{Col}$ being heterozygous with $Ws\text{-}4^{Bur}$. As in the creation of $Ws\text{-}4^{Col}$
304 no plant was used with a Bur plasmotype, this suggested a sample mix-up. To confirm such, and that
305 the putative event of cross-contamination had occurred in the laboratory, we designed seven KASP™
306 makers (LGC, https://www.lgcgroup.com) to genotype all cybrids. These KASP™ markers are
307 designed to be unique for the chloroplast allele of one accession, and target SNPs that were called as
308 heterozygous in the sequence analysis (Supplementary Table 7). The KASP™ assay can distinguish
309 between homozygous and heterozygous states. We assayed all seven KASP™ markers on all cybrids,
310 for $C24^{C24}$ and $Ws\text{-}4^{Col}$ this included plants from the same seed batch as the plants used for
311 sequencing, as well as direct offspring of the sequenced plants. All lines showed to be the genotypes
312 as predicted, and no chloroplast heterozygosity was observed in any of the lines, including $C24^{C24}$ and
313 $Ws\text{-}4^{Col}$ (Supplementary Table 8). Unfortunately, the Ely^{Sha} used for sequencing died before setting
314 seed and although it has since been recreated, it could not be included in our phenotypic analyses.
315 We have used the KASP™ marker for the Sha chloroplast, and confirmed it to be correct
316 (Supplementary Table 8).

317 To check for any incomplete chromosome eliminations, we calculated the read coverage for
318 all cybrids, normalized per chromosome. We did not observe any remaining chromosomes, however
319 we did detect a 200-kb duplication of chromosome 2 nuclear DNA in Bur^{C24} and the self-cybrid Bur^{Bur}.
320 As the exact same duplicated segment is present in two independent cybrid lines and is a duplication
321 of Bur nuclear origin (based on sequence identity), we conclude this segment results from a *de-novo*
322 duplication in one of the wild-type Bur lines used to generate these two cybrids. Following the

exclusion of phenotyping data for Bur^{Bur} and Bur^{C24} we limited our analyses to 46 rather than 49 cybrids. The parental lines were included in the screens to test for possible unforeseen effects of cybrid production (which involves a haploid growth stage). This brings the number of phenotyped lines in this study to a total of 53 (40 cybrids, 6 self-cybrids and 7 wild types).

The fuctional effects of the chloroplastic and mitochondrial SNPs and INDELs were predicted using SnpEff [24]. A SnpEff database was built using the genome, transcriptome and proteome as released in TAIR10.1. SNPs and INDELs were predicted on the filtered VCF, as mentioned above. In the analysis we only considered varaints with a "HIGH" or "MODERATE" impact.

Phenotyping: Cybrids were phenotypically assessed using different platforms. For details on the number of phenotypes per experiment see Supplementary Table 4.

Growth, PSII efficiency (Φ_{PSII}), chlorophyll reflectance and leaf movement (all parameters at n=24) was screened in the Phenovator platform, a high-throughput phenotyping facility located in a climate-controlled growth chamber [47]. This phenotyping platform measured the plants for: Φ_{PSII} using chlorophyll fluorescence, reflectance at 480 nm, 532 nm, 550 nm, 570 nm, 660 nm, 700 nm, 750 nm and 790 nm, and projected leaf area (PLA) based on pixel counts of near infra-red (NIR) images [47]. The growth chamber was set to a 10 h day/14 h night regime, at 20°C day and 18°C night temperature, 200 µmol m^{-2} s^{-1} irradiance, and 70% relative humidity. The plants were grown on a rockwool substrate and irrigated daily with a nutrient solution as described in Flood, et al. [47].

Growth (n=24) and subsequently above ground biomass (n=12) was measured in another high-throughput phenotyping facility [48], where projected leaf area was measured three times per day with 14 fixed cameras (uEye Camera, IDS Imaging Development Systems GmbH, Obersulm, Germany). This growth chamber was set to a 10 h day/14 h night regime, at 20°C day and 14°C night temperature, 200 µmol m^{-2} s^{-1} light and 70% relative humidity. Plants were grown on rockwool and irrigated weekly with a nutrient solution as described before.

Non-fluctuating and fluctuating light treatments were performed in the DEPI phenotyping facility of Michigan State University (n=4)[49]. This facility is able to measure the chlorophyll fluorescence derived photosynthetic parameters, Φ_{PSII}, Φ_{NO}, Φ_{NPQ}, NPQ, q_E, q_I. Three-week-old plants were moved into the facility, where they were left to acclimatize for 24 hours after which three days of phenotyping was performed under different light regimes. On the first day the plants were illuminated

with a constant light intensity of 200 µmol m^{-2} s^{-1}. On the second day the plants received a sinusoidal light treatment where the light intensity began low and gradually increased to a maximum of 500 µmol m^{-2} s^{-1} light from which it deceased back down to 0. On the third day the plants received a fluctuating light treatment ranging between 0 and 1000 µmol m^{-2} s^{-1} light in short intervals (Fig. 3c). For the second experiment in the DEPI phenotyping facility the experiment was extent with 2 days, in which day 4 replicated day 2 and day 5 replicated day 2 (Supplementary Data 1 and Extended Data Fig. 7c). For further details see Cruz, et al. [49].

Bolting time and flowering time were measured on all cybrids (n=10) in a greenhouse experiment in April 2017, with the exception of Ely nucleotype cybrids which needed vernalisation and were not included in this experiment. Additional lighting was turned on when the natural light intensity fell below 685.5 µmol m^{-2} s^{-1}, and turned off when the light intensity reached 1142.5 µmol m^{-2} s^{-1}, with a maximum of 16 h per day.

Seeds for the germination experiments were generated from two rounds of propagation. In the first-round seeds were first sown in a growth chamber set to a 10 h day/14 h night regime, at 20°C day and 18°C night temperature. 200 µmol m^{-2} s^{-1} light intensity, and 70% relative humidity. After three weeks they were moved to an illuminated cold room at 4°C for six weeks of vernalization. After vernalization all plants (n=8) were moved to a temperature-controlled greenhouse (20°C) for flowering and seed ripening. Exceptions to this were L*er*^{Ely}, L*er*$^{Ws\text{-}4}$, and Ely$^{Ws\text{-}4}$ for which no doubled haploid seed was available at the beginning of the first propagation round. L*er*^{Ely} and L*er*$^{Ws\text{-}4}$ were sown later, during the vernalization stage and flowered at the same time as the vernalized plants. Ely$^{Ws\text{-}4}$ produced haploid seed at a later stage and could not be included in the first propagation round. Plants were grown in a temperature-controlled greenhouse set at 20°C. In this round only lines with the Ely nucleotype were vernalized. For the germination experiments seeds were stratified on wet filter paper for four days at 4°C before being assayed in the Germinator platform [50] for seed size, germination rate and total germination percentage. Germination under osmotic stress was performed on filter paper with 125 mM NaCl. For the controlled deterioration treatment, seeds were incubated for 2.5, 5 or 7 days at 40°C and 82% RH and subsequently assayed in the Germinator platform without stratification.

To assess pollen abortion all cybrid lines and wild-type progenitors (except those with the Ely nucleotype) were grown simultaneously in a growth chamber (Percival) under controlled conditions (16H/ 8H light cycle, 21º/18º ºC and 50%-60% relative humidity). Pollen abortion was manually

assessed for all the genotypes by using a differential staining of aborted and non-aborted pollen grains [51]. A total of three plants and three flowers per plant of each cybrid were collected on the same day and submerged in a drop of 13 µl of phenol-free Alexander staining solution placed on a glass slide with a glass cover slip of 18x18 mm. For each flower 250 pollen grains were counted and the number of aborted pollen therein.

Oxygen consumption of seedlings was measured in 2 mL of deionized water with a liquid-phase Oxytherm oxygen electrode system (Hansatech Instruments) calibrated at the measurement temperature. Three-day-old seedlings (about 50 mg) were directly imbibed in the electrode chamber. The rates of oxygen consumption were measured after tissue addition and subtracted from the rates after addition of 500 µM KCN. Results are the mean of at least five measurements. Measurements for different genotypes were performed on consecutive days, and to correct for daily variation, normalized to Col-0 samples that were run daily.

Metabolomics: Plant material for primary metabolite analysis was obtained from the 'Phenovator' photosynthetic phenotyping experiment. Plants were harvested 26 days after sowing, which due to the 10-hr photoperiod was prior to bolting for all lines. Samples were frozen in liquid nitrogen, and samples of each genotype were subsequently combined into four pools each made up of material of approximately six replicates. Each pool was ground and homogenized before an aliquot was taken for further analysis. Reference samples for the metabolite analysis were composed of material from all seven parents in equal amounts and then homogenized. The method used for the extraction of polar metabolites from *Arabidopsis* leaves was adapted from Lisec, et al. [52] as described by Carreno-Quintero, et al. [53]. Specific adjustments for *Arabidopsis* samples were made as follows; the polar metabolite fractions were extracted from 100 mg of *Arabidopsis* leaf material (fresh weight, with max. 5% deviation). After the extraction procedure, 100-µL aliquots of the polar phase were dried by vacuum centrifugation for 16 hours. The derivatization was performed on-line similar as described by Lisec, et al. [52] and the derivatized samples were analyzed by a GC-ToF-MS system composed of an Optic 3 high-performance injector (ATAS^{TM}, GL Sciences, Eindhoven, The Netherlands) and an Agilent 6890 gas chromatograph (Agilent Technologies, Santa Clara, California, United States) coupled to a Pegasus III time-of-flight mass spectrometer (Leco Instruments, St. Joseph, Michigan, United States). Two microliters of each sample were introduced in the injector at 70°C using 5% of the

sample (split 20). The detector voltage was set to 1750 Volts. All samples were analyzed in random order in four separate batches. The systematic variation that inadvertently is introduced by working in batches, was removed upon analysis of covariance. In this model the batch number was used as a factor (four levels) and "run number within a batch" as a covariate since it is also expected that (some) variation will be introduced by the sample run order within each batch. For this the S2 method described by [54] was used to perform the least-squares regression. After quality control and removing metabolites with more than 20% missing data and a broad sense heritability (H^2) of less than 5%, we were left with data on 41 primary metabolites. Metabolites were identified based on the Level of Identification Standard of the Metabolomics Standards Initiative [55].

Transcriptome analysis: Using the same material as described in the metabolome analysis, total RNA was extracted from six cybrids, three in a L*er* and three in an Ely nuclear background: Ler^{Ler} Ler^{Ely}, Ler^{Bur} and Ely^{Ler} Ely^{Ely}, Ely^{Bur} with three replicates per genotype, totaling 18 plants. Library preparation was done with a selection on 3' polyadenylated tails to preferentially include nuclear mRNA. Read alignment was done using TopHat [56]. Any chloroplast and mitochondrial genes remaining were excluded from further analysis. The raw counts were normalized and analyzed using the DeSeq2 package in R [57]. Genes for which the expression levels were significantly different between two cybrids were determined by comparing two genotypes using the contrast function of DeSeq2. P-values were determined using the Wald test, and p-values were adjusted using the Benjamini-Hochberg correction (α=0.05). GO enrichment analysis was done using default setting in g:profiler (g:GOSt). The complete set of detected genes in each cybrid was used as a statistical background in the analysis [58].

Phenotypic data analysis: We used the self-cybrids as our baseline in phenotypic comparisons to control for any possible effects of cybrid creation, with the exception of Bur^{Bur} which was replaced in all analysis with Bur-WT. Raw data were directly analyzed except for time series data of growth and chlorophyll reflectance which were preprocessed as follows. Time series data were fitted with a smooth spline using the gam function from the mgcv package in R [59]. The fitted B-spline was subsequently used to derive curve parameters. These include area under the curve, slope under mean, first, second (median) and third quartile, minimal and maximal slope, and the timepoint where the slope is maximum. These parameters allow us to quantify not only plant size and growth rate but

also the dynamic properties of the growth curve, i.e. did growth occur early, late, or constant through time. In addition, we calculated relative growth rate per time point by dividing the growth rate, relative to the plant size [47]. All raw parameters and derived parameters were analyzed by fitting either a linear mixed model or a linear model. The linear mixed model was used when a random correction parameter was present, when such random correction parameters were absent a linear model was used. The models were analyzed using the Restricted Maximum Likelihood (REML) procedure for each relevant phenotype using the lme4 package in R [60]. As each experiment had a different design, several models were employed (Supplementary Table 4). The following model was generally used, in some instances random terms (underlined below) were added:

$$\underline{Y} = Nucleotype + Plasmotype + (Nucleotype * Plasmotype) + \underline{Block} + \underline{\varepsilon} \qquad (1)$$

For every model, normality and equal variances were checked. Next, for every phenotypic parameter we calculated significant difference for the plasmotype and interaction term of the model (equation 1). This was done by ANOVA in which Kenward-Roger approximation for degrees of freedom was used. As posthoc tests we used a two-sided Dunnett's test, where we tested whether a given cybrid was different from the self-cybrid control, within one nucleotype. Two-side Hochberg's posthoc tests were used when all pairwise comparisons were tested within one nucleotype (to test for epistasis) and across all nucleotypes (to test for additivity). The significance threshold for all posthoc tests was set at α=0.05. The contribution of the nucleotype, plasmotype and the interaction between the two, was determined by estimating the variance components in mixed models containing the same terms as in model (1). However, the fixed terms were taken as random:

$$\underline{Y} = \underline{Nucleotype} + \underline{Plasmotype} + \underline{(Nucleotype * Plasmotype)} + \underline{Block} + \underline{\varepsilon},$$

In this model the variance components were estimated by the VarCorr function from the lme4 package. Total variance was calculated by summing all the variance components, after which the fraction explained variance for every term in the model was calculated. The broad sense heritability, in our case equal to repeatability (Falconer and Mackay, 1996), is determined by the three genetic

components, i.e. nucleotype, plasmotype and their interaction. The fraction of broad sense heritability explained by the separate genetic components was calculated subsequently.

In total we measured 1859 phenotypes. After data processing, further analysis was only conducted on phenotypes with a broad sense heritability higher than 5%, removing phenotypes that were non-informative, leaving us with 1782 phenotypes. Furthermore, to avoid biases in the results due to overly correlated data when stating summary statistics, we further subset the remaining 1782 phenotypes (Supplementary Data 2). Using a threshold based purely on correlation would favor the inclusion of variation largely driven by the nucleotype. Since the population is balanced, we subtracted the averages of the nucleotype values from the cybrid phenotype values, to reveal the plasmotype effect per cybrid. From these we calculated the Pearson correlations for all phenotypes. This highlighted that the most uncorrelated phenotypes mainly stem from one experiment assessing photosynthetic parameters under fluctuating light. The unbiased selection of a subset of phenotypes would result in the omission of several phenotypic categories. To present a balanced overview of all phenotypic categories we manually selected a subset comprising the following phenotypes. For time series in which we scored for up to 25 days after germination, we selected the morning measurements of day 8, 13, 18 and 23. The time series analysis of fluctuating light were measured for three (first experiment, Fig. 3) and five days (replicate experiment; Extended Data Fig. 7) in a row, with each day subjected to a different treatment. As these treatments reached their extremes in the middle and at end of the day, and the results of replicate experiments were very similar, we selected time points in the middle and at the end of the day of only the first experiment. For the different seed treatments we used the germination time until 50% of the seeds germinated. In addition, we included biomass, leaf movement, seed size, flowering time as single phenotypes and all 36 primary metabolites. This resulted in 92 phenotypes, that are used for giving summary and test statistics (for a correlation plot of these, please see Extended Data Fig. 3). All data on the 1859 phenotypes, with summary and test statistics are available in Supplementary Data 1 and Supplementary Table 3.

The correlation between plasmotype additive and plasmotype epistatic effects was calculated with and without the Ely plasmotype. For both additive and epistatic effects every significant change between plasmotypes, within one nucleotype background, was counted (Supplementary Data 2). The Pearson correlation coefficients and accompanying p-values were calculated using the ggpubr package in R.

References:

1. Ravi, M. *et al.* A haploid genetics toolbox for *Arabidopsis thaliana*. *Nature Communications* **5**, 5334 (2014).
2. Chan, K.X., Phua, S.Y., Crisp, P., McQuinn, R. & Pogson, B.J. Learning the Languages of the Chloroplast: Retrograde Signaling and Beyond. *Annual Review of Plant Biology* **67**, 25-53 (2016).
3. Petrillo, E. *et al.* A Chloroplast Retrograde Signal Regulates Nuclear Alternative Splicing. *Science* **344**, 427-430 (2014).
4. Kleine, T. & Leister, D. Retrograde signaling: Organelles go networking. *Biochimica et Biophysica Acta (BBA) - Bioenergetics* **1857**, 1313-1325 (2016).
5. Flood, Pádraic J. *et al.* Whole-Genome Hitchhiking on an Organelle Mutation. *Current Biology* **26**, 1306-1311 (2016).
6. Joseph, B., Corwin, J.A., Li, B., Atwell, S. & Kliebenstein, D.J. Cytoplasmic genetic variation and extensive cytonuclear interactions influence natural variation in the metabolome. *eLife* **2**, e00776 (2013).
7. Zeyl, C., Andreson, B. & Weninck, E. Nuclear-mitochondrial epistasis for fitnes in *Saccharomyces cerevisiae*. *Evolution* **59**, 910-914 (2005).
8. Montooth, K.L., Meiklejohn, C.D., Abt, D.N. & Rand, D.M. Mitochondrial-nuclear epistasis affects fitness within species but does not contribute to fixed incompatibilities between species of *Drosophila*. *Evolution* **64**, 3364-3379 (2010).
9. Joseph, B. *et al.* Hierarchical Nuclear and Cytoplasmic Genetic Architectures for Plant Growth and Defense within Arabidopsis. *The Plant Cell Online* **25**, 1929-1945 (2013).
10. Tang, Z. *et al.* Potential Involvement of Maternal Cytoplasm in the Regulation of Flowering Time via Interaction with Nuclear Genes in Maize. *Crop Science* **54**, 544-553 (2014).
11. Roux, F. *et al.* Cytonuclear interactions affect adaptive traits of the annual plant *Arabidopsis thaliana* in the field. *Proceedings of the National Academy of Sciences* **113**, 3687-3692 (2016).
12. Mossman, J.A., Ge, J.Y., Navarro, F. & Rand, D.M. Mitochondrial DNA Fitness Depends on Nuclear Genetic Background in *Drosophila*. *G3: Genes, Genomics, Genetics* **9**, 1175-1188 (2019).
13. Dobler, R., Rogell, B., Budar, F. & Dowling, D.K. A meta-analysis of the strength and nature of cytoplasmic genetic effects. *J. Evolution Biol.* **27**, 2021-2034 (2014).
14. Bock, D.G., Andrew, R.L. & Rieseberg, L.H. On the adaptive value of cytoplasmic genomes in plants. *Mol. Ecol.* **23**, 4899-4911 (2014).
15. Levings, C.S. The Texas Cytoplasm of Maize: Cytoplasmic Male Sterility and Disease Susceptibility. *Science* **250**, 942-947 (1990).
16. Miclaus, M. *et al.* Maize Cytolines Unmask Key Nuclear Genes That Are under the Control of Retrograde Signaling Pathways in Plants. *Genome Biology and Evolution* **8**, 3256-3270 (2016).
17. Sambatti, J.B., Ortiz-Barrientos, D., Baack, E.J. & Rieseberg, L.H. Ecological selection maintains cytonuclear incompatibilities in hybridizing sunflowers. *Ecology letters* **11**, 1082-1091 (2008).
18. Dowling, D.K., Abiega, K.C. & Arnqvist, G. Temperature-specific outcomes of cytoplasmic-nuclear interactions on egg-to-adult development time in seed beetles. *Evolution* **61**, 194-201 (2007).
19. Ravi, M. & Chan, S.W.L. Haploid plants produced by centromere-mediated genome elimination. *Nature* **464**, 615-618 (2010).
20. El-Lithy, M.E. *et al.* Altered photosynthetic performance of a natural *Arabidopsis* accession is associated with atrazine resistance. *Journal of Experimental Botany* **56**, 1625-1634 (2005).
21. Flood, P.J. *et al.* Natural variation in phosphorylation of photosystem II proteins in Arabidopsis thaliana: is it caused by genetic variation in the STN kinases? *Philosophical Transactions of the Royal Society B: Biological Sciences* **369**(2014).
22. Falconer, D. & Mackay, T.J.H., Essex, UK: Longmans Green. Introduction to quantitative genetics. 1996. **3**(1996).

23. Somerville, C.R. & Ogren, W.L. Photorespiration mutants of *Arabidopsis thaliana* deficient in serine-glyoxylate aminotransferase activity. *Proceedings of the National Academy of Sciences* **77**, 2684-2687 (1980).
24. Cingolani, P. *et al.* A program for annotating and predicting the effects of single nucleotide polymorphisms, SnpEff. *Fly* **6**, 80-92 (2012).
25. Kermicle, J.L. Androgenesis Conditioned by a Mutation in Maize. *Science* **166**, 1422-1424 (1969).
26. Schneerman, M., Charbonneau, M. & Weber, D. A survey of ig containing materials. *Maize Genetics Cooperation Newsletter*, 54-55 (2000).
27. Houben, A., Sanei, M. & Pickering, R. Barley doubled-haploid production by uniparental chromosome elimination. *Plant Cell, Tissue and Organ Culture* **104**, 321-327 (2011).
28. Karimi-Ashtiyani, R. *et al.* Point mutation impairs centromeric CENH3 loading and induces haploid plants. *Proceedings of the National Academy of Sciences* **112**, 11211-11216 (2015).
29. Kromdijk, J. *et al.* Improving photosynthesis and crop productivity by accelerating recovery from photoprotection. *Science* **354**, 857-861 (2016).
30. Flood, P.J., Harbinson, J. & Aarts, M.G.M. Natural genetic variation in plant photosynthesis. *Trends Plant Science* **16**, 327-335 (2011).
31. Murchie, E.H. *et al.* Measuring the dynamic photosynthome. *Annals of Botany* **122**, 207-220 (2018).
32. Ruf, S. *et al.* High-efficiency generation of fertile transplastomic Arabidopsis plants. *Nature Plants* **5**, 282-289 (2019).
33. Kwak, S.-Y. *et al.* Chloroplast-selective gene delivery and expression in planta using chitosan-complexed single-walled carbon nanotube carriers. *Nature Nanotechnology* **14**, 447-455 (2019).
34. Zhang, J. *et al.* Full crop protection from an insect pest by expression of long double-stranded RNAs in plastids. *Science* **347**, 991-994 (2015).
35. Jin, S. & Daniell, H. The Engineered Chloroplast Genome Just Got Smarter. *Trends in Plant Science* **20**, 622-640 (2015).
36. Hoekstra, L.A., Siddiq, M.A. & Montooth, K.L. Pleiotropic effects of a mitochondrial–nuclear incompatibility depend upon the accelerating effect of temperature in Drosophila. *Genetics* **195**, 1129-1139 (2013).
37. Mossman, J.A., Biancani, L.M., Zhu, C.-T. & Rand, D.M. Mitonuclear epistasis for development time and its modification by diet in Drosophila. *Genetics* **203**, 463-484 (2016).
38. Hill, G.E. *et al.* Assessing the fitness consequences of mitonuclear interactions in natural populations. *Biological Reviews* **94**, 1089-1104 (2019).
39. Yin, L. *et al.* Photosystem II Function and Dynamics in Three Widely Used *Arabidopsis thaliana* Accessions. *PLoS ONE* **7**, e46206 (2012).
40. Gobron, N. *et al.* A Cryptic Cytoplasmic Male Sterility Unveils a Possible Gynodioecious Past for *Arabidopsis thaliana*. *PLoS ONE* **8**, e62450 (2013).
41. Wijnker, E. *et al.* Hybrid recreation by reverse breeding in Arabidopsis thaliana. *Nature protocols* **9**, 761-772 (2014).
42. Martin, M. Cutadapt removes adapter sequences from high-throughput sequencing reads. *EMBnet. journal* **17**, 10-12 (2011).
43. Sloan, D.B., Wu, Z. & Sharbrough, J. Correction of persistent errors in Arabidopsis reference mitochondrial genomes. *The Plant Cell*, tpc. 00024.2018 (2018).
44. Li, H. Aligning sequence reads, clone sequences and assembly contigs with BWA-MEM. in *arXiv e-prints* (2013).
45. Li, H. *et al.* The Sequence Alignment/Map format and SAMtools. *Bioinformatics* **25**, 2078-2079 (2009).
46. The 1001 Genomes Consortium. 1,135 Genomes Reveal the Global Pattern of Polymorphism in Arabidopsis thaliana. *Cell*, 481-491 (2016).

47. Flood, P.J. *et al.* Phenomics for photosynthesis, growth and reflectance in Arabidopsis thaliana reveals circadian and long-term fluctuations in heritability. *Plant Methods* **12**, 1-14 (2016).
48. Kokorian, J., Polder, G., Keurentjes, J., Vreugdenhil, D. & Guzman, M.O. An ImageJ based measurement setup for automated phenotyping of plants. in *Proceedings of the ImageJ User and Developer Conference, Luxembourg, Luxembourg, 27-29 October 2010* 178-182 (2010).
49. Cruz, J.A. *et al.* Dynamic Environmental Photosynthetic Imaging Reveals Emergent Phenotypes. *Cell Systems* **2**, 365-377 (2016).
50. Joosen, R.V.L. *et al.* germinator: a software package for high-throughput scoring and curve fitting of Arabidopsis seed germination. *The Plant Journal* **62**, 148-159 (2010).
51. Peterson, R., Slovin, J.P. & Chen, C.J.I.J.o.P.B. A simplified method for differential staining of aborted and non-aborted pollen grains. *International Journal of Plant Biology* **1**, e13-e13 (2010).
52. Lisec, J., Schauer, N., Kopka, J., Willmitzer, L. & Fernie, A.R. Gas chromatography mass spectrometry-based metabolite profiling in plants. *Nature Protocols* **1**, 387-396 (2006).
53. Carreno-Quintero, N. *et al.* Untargeted Metabolic Quantitative Trait Loci Analyses Reveal a Relationship between Primary Metabolism and Potato Tuber Quality. *Plant Physiology* **158**, 1306-1318 (2012).
54. Wehrens, R. *et al.* Improved batch correction in untargeted MS-based metabolomics. *Metabolomics* **12**, 88 (2016).
55. Sumner, L.W. *et al.* Proposed minimum reporting standards for chemical analysis. *Metabolomics* **3**, 211-221 (2007).
56. Trapnell, C., Pachter, L. & Salzberg, S.L. TopHat: discovering splice junctions with RNA-Seq. *Bioinformatics* **25**, 1105-1111 (2009).
57. Love, M.I., Huber, W. & Anders, S. Moderated estimation of fold change and dispersion for RNA-seq data with DESeq2. *Genome Biology* **15**, 550 (2014).
58. Reimand, J. *et al.* g:Profiler—a web server for functional interpretation of gene lists (2016 update). *Nucleic Acids Research* **44**, W83-W89 (2016).
59. Wood, S.N., Pya, N. & Säfken, B. Smoothing Parameter and Model Selection for General Smooth Models. *Journal of the American Statistical Association* **111**, 1548-1563 (2016).
60. Bates, D., Mächler, M., Bolker, B. & Walker, S. Fitting linear mixed-effects models using lme4. *Journal of Statistical Software* **67**, 48 (2015).

Corresponding authors: Correspondence and requests for materials can be addressed to P.J. Flood (flood@mpipz.mpg.de), T.P.J.M. Theeuwen (tom.theeuwen@wur.nl), and E. Wijnker (erik.wijnker@wur.nl).

Acknowledgements: Hetty Blankestijn, Jose van de Belt, Daniel Oberste-Lehn, Elio Schijlen, Corrie Hanhart, Joris ter Riele and Sharella Schop (Wageningen University & Research) are acknowledged for help with experiments, Jonas Klasen (Max Planck Institute for Plant Breeding Research), Antoine Languillaume and Roel van Bezouw (Wageningen University & Research) for statistical advice, and Duur Aanen (Wageningen University & Research) for helpful discussions. The authors would also like to thank four reviewers whose input greatly improved the manuscript. This work was in part supported by the Netherlands Organization for Scientific Research (NWO) through ALW-TTI Green Genetics (P.J.F.), ALWGS.2016.012 (T.P.J.M.T) and STW-14389 (E.W.). The European Molecular Biology Organization supported through ALTF 679-2013 (E.W.) and the European Community (EC) though the Marie-Curie Initial Training Network “COMREC”, project 606956 funded under FP7-PEOPLE (V.C.-B.). ZonMw Enabling Technology Hotels and the Consortium for Improving Plant yield (CIPY) Enabling Technology Hotels provided funds for the metabolomics, RNA-seq and seed phenotyping. Work at MSU for DEPI phenotyping was supported by the U.S. Department of Energy (DOE), Chemical Sciences, Geosciences, and Biosciences Division, Basic Energy Sciences, Office of Science at the U.S. Department of Energy (through grant DE-FG02–91ER20021).

Author contributions: P.J.F. and E.W. conceived and designed the study. T.P.J.M.T. designed and performed the statistical analysis with help from P.J.F., W.K. and F.v.E.. P.J.F., T.P.J.M.T., E.K., F.F.M.B., L.A.J.W., V.C.B., J.v.A., J.M.G., and L.S. performed experiments. P.J.F., T.P.J.M.T., K.S., P.K., E.S., J.A.H., S.K.S., R.W., W.L., R.M., F.v.E. and E.W. analysed data. D.M.K., J.J.B.K., M.K., J.H. and M.G.M.A. contributed to the interpretation of results. P.J.F., T.P.J.M.T. and E.W. wrote the paper with significant contributions from M.K., J.H. and M.G.M.A. All authors read and approved the final manuscript.

Competing interests statement: The authors declare no competing interests

Data availability: Sequencing and transcriptome data are available through the European Nucleotide Archive with the primary accession codes PRJEB29654 and PRJEB35324. The raw datasets are available through Dryad via doi:10.5061/dryad.cz8w9gj05. The analysed datasets that support our findings are available as Supplementary Data. The associated raw data for Figs. 2 and 3 are provided in Supplementary Data 1, the raw data for Table 1 is provided in Supplementary Data 2. The germplasm generated in this project will be available via the European Arabidopsis Stock Centre (www.arabidopsis.info).

Figure and table legends:

Fig. 1: Generation of a cybrid test panel. a, Generation of a new haploid inducer (HI) line with a new plasmotype. The HI expresses a GFP-tagged *CENH3/HRT12* in a *cenh3/htr12* mutant background. A cross of a wild type (female) with a HI (male) results in a hybrid F1. A diploid F1 is selected in which no genome elimination has occurred. Self-fertilization generates an F2 population in the plasmotype of the wild-type mother. From this an F2 plant is selected that is homozygous for the *cenh3/htr12* mutation and carries the *GFP-tailswap* transgene. This F2 plant is a new HI line and can serve as plasmotype donor when used as female in crosses. Vertical bars represent the nucleotype, and the ovals represent the plasmotype. HI centromeres are indicated in green (signifying GFP-tagged CENH3/HTR12 proteins as encoded by the *GFP-tailswap* construct) that cause uniparental genome-elimination. **b**, HI lines can function as plasmotype donors when used as a female parent. In this case, uniparental genome elimination (red arrow) leads to a haploid offspring plant with the nucleotype of the wild-type (WT) male parent, but the plasmotype of the HI mother. **c**, Full diallel of all nucleotype-plasmotype combinations for which cybrids were generated. The diagonal line highlights the wild-type (WT) nucleotype-plasmotype combinations that were generated by crossing wild-type plants to plasmotype donors with the plasmotype of the wild type (self-cybrids). Bur^{Bur}, Bur^{C24} and Ely^{Sha} are faded, as they were not included in the phenotyping experiments, but have been subsequently recreated.

Fig. 2: Plasmotype changes result in cytonuclear epistasis, and in the case of cybrids with the Ely and Bur plasmotype also in additive effects. a, Pollen abortion, percentage of dead pollen out of 250. **b**, PSII efficiency (Φ_{PSII}) 71.46 hours after start of experiment, after a full day of fluctuating light

with a maximum difference between 500 and 100 µmol/m^2/s irradiance (see Fig. 3c for light treatment). **c**, NPQ at 38.46 hours after start of experiment, which is at 300 µmol/m^2/s on a sigmoidal light curve starting at 65 µmol/m^2/s. **d**, The rapidly reversible component of NPQ, q_E, at 259 µmol/m^2/s after a full day of fluctuating light with a maximum difference between 500 and 100µmol/m^2/s. X-axis are labelled with the plasmotype, and the colours represent the nucleotypes. Any deviation from a horizontal line represents a potential additive or epistatic effect. Error bars represent the standard error of the mean. The asterisk (*) in panel **a** indicates a unique significant difference between the Sha^{Sha} cybrid and other cybrids with Sha nucleotypes (epistasis) (Hochberg's test, n=minimally 4 biologically independent plants, for exact p-values see Supplementary Data 1). The letters above panels **b**, **c** and **d** represent significant differences between plasmotypes regardless of the nucleotype (additivity) (Hochberg's test, n=4 biologically independent cybrids *7 different nucleotypes, letters are different when α=0.05). For panels **b**, **c** and **d** plants were grown at 200 µmol m^{-2} s^{-1} light intensity for 21 days prior to starting the experiment.

Fig. 3: The fraction of explained genetic variation (H^2) for photosynthesis phenotypes differs depending on light conditions. a, Shows the fraction of H^2 for plasmotype epistatic effects. **b**, Shows the fraction of H^2 for plasmotype additive effects. **c**, Shows the light intensity for three consecutive days with growth under steady light (day 1), sinusoidal light intensity (day 2) and fluctuating light intensity (day 3). Days are separated by nights (shaded areas). Note that the fraction of H^2 for different phenotypes changes markedly during days 2 and 3. Some phenotypes are explained largely by additive effects (i.e. q_E) while others by interaction (i.e. Φ_{NPQ}). A replication of this experiment is shown in Extended Data Fig. 7.

Table 1. Significant plasmotype induced effects in 92 phenotypes. a, The number of observed significant plasmotype additive effects when a specific plasmotype is changed for another plasmotype, regardless of the nucleotype. Note that the replacement of Bur (top row) and Ely plasmotypes (last column) result in most plasmotype additive effects. **b**, The number of observed significant epistatic effects in phenotypes between wild-type nucleotype-plasmotype combinations and cybrids with different plasmotypes. Rows indicate the number of significant effects when comparing self-cybrids to cybrids with identical nucleotype but non-native plasmotype. Columns indicate specific plasmotype

changes. Note that changing the Ely plasmotype for another plasmotype (bottom row and last column) results in many epistatic effects due to the large-effect mutation in the chloroplast-encoded *PsbA* gene of the Ely plasmotype. Similar effects, but of smaller magnitude, result from changing the Bur plasmotype (top row and first column). Posthoc tests were used with Hochberg's p-value correction for panel a and Dunnett's p-value correction (with the wild-type as control) for panel b, α=0.05. nd = not determined. For underlying p-values and phenotypes see Supplementary Data 2. Orange cells indicate a low number of significant effects; blue cells show a high number of significant effects.

Table 1a

# of significant phenotypes 0–55			Plasmotype						
			XXX^{Bur}	XXX^{C24}	XXX^{Col}	XXX^{Ler}	XXX^{Sha}	XXX^{Ws-4}	XXX^{Ely}
Table 1a	Plasmotype	XXX^{Bur}		12	15	10	15	6	55
		XXX^{C24}			1	0	1	0	50
		XXX^{Col}				2	2	1	50
		XXX^{Ler}					0	1	48
		XXX^{Sha}						2	49
		XXX^{Ws-4}							49
		XXX^{Ely}							

Table 1b

# of significant phenotypes 0–48			Plasmotype						
			XXX^{Bur}	XXX^{C24}	XXX^{Col}	XXX^{Ler}	XXX^{Sha}	XXX^{Ws-4}	XXX^{Ely}
Table 1b	Wild-type nucleotype-plasmotype combination	Bur wildtype		nd	4	7	9	4	48
		C24^{C24}	4		1	0	3	1	32
		Col^{Col}	5	2		0	1	1	39
		L*er*^{Ler}	0	0	1		3	6	37
		Sha^{Sha}	10	2	1	1		2	40
		Ws-4^{Ws-4}	4	3	0	0	4		37
		Ely^{Ely}	41	45	44	42	nd	42	

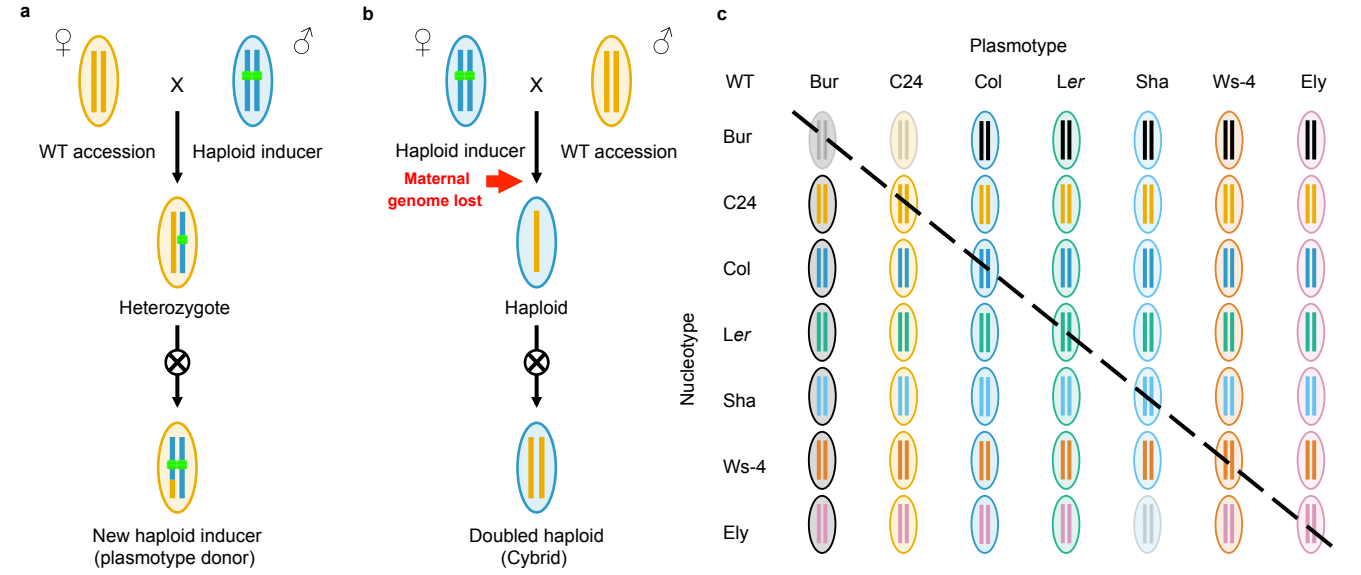
a
WT accession
X
Haploid inducer
Heterozygote
New haploid inducer
(plasmotype donor)
b
Haploid inducer
X
WT accession
Maternal
genome lost
Haploid
Doubled haploid
(Cybrid)
c
Plasmotype
WT
Bur
C24
Col
Ler
Sha
Ws-4
Ely
Nucleotype

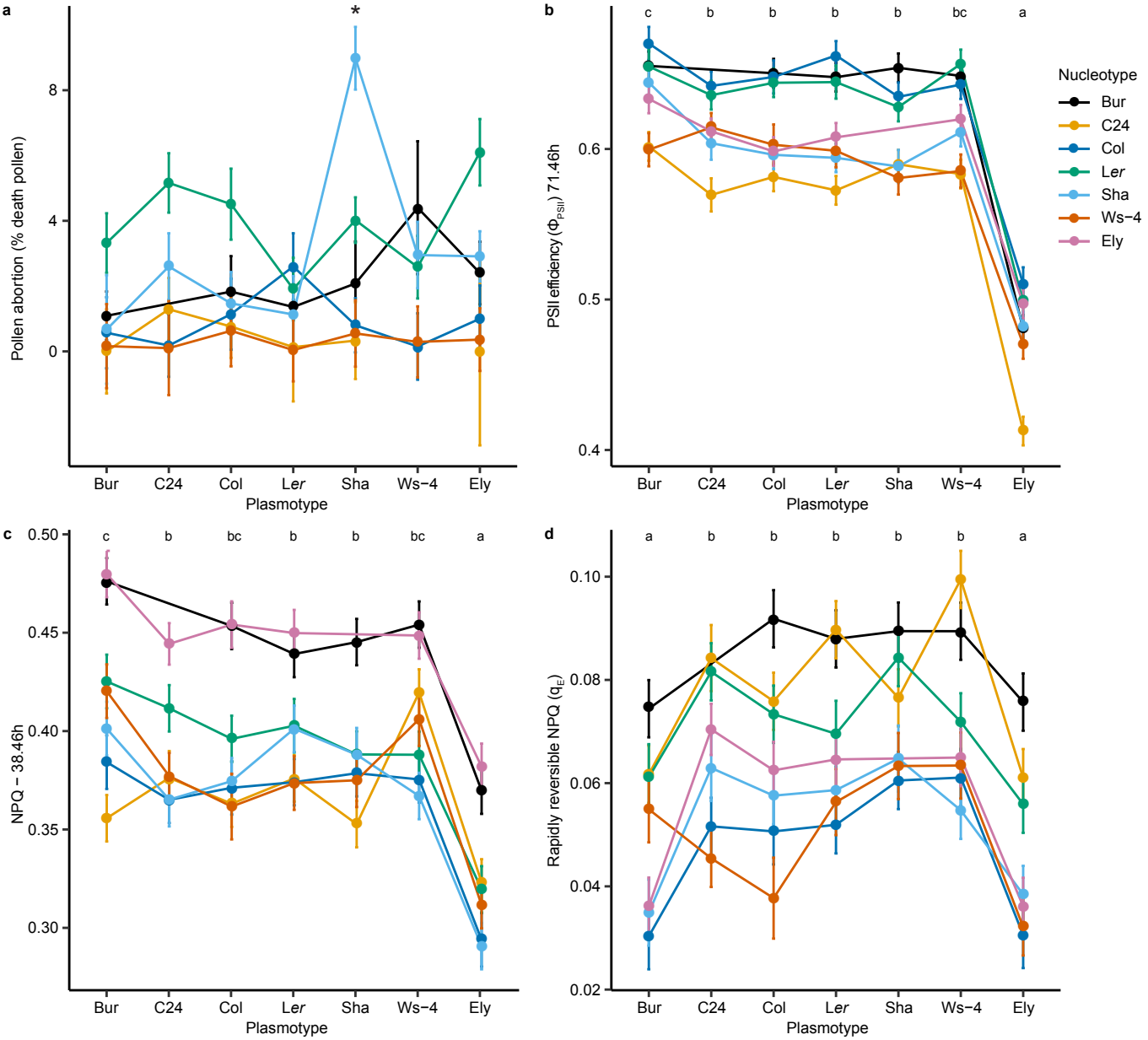
a
Pollen abortion (% death pollen)
8
4
0
*
Bur
C24
Col
Ler
Sha
Ws−4
Ely
Plasmotype
b
PSII efficiency (Φ_{PSII}) 71.46h
0.6
0.5
0.4
c b b b b bc a
Bur
C24
Col
Ler
Sha
Ws−4
Ely
Plasmotype
Nucleotype
Bur
C24
Col
Ler
Sha
Ws−4
Ely
c
NPQ − 38.46h
0.50
0.45
0.40
0.35
0.30
c b bc b b bc a
Bur
C24
Col
Ler
Sha
Ws−4
Ely
Plasmotype
d
Rapidly reversible NPQ (q_E)
0.10
0.08
0.06
0.04
0.02
a b b b b b a
Bur
C24
Col
Ler
Sha
Ws−4
Ely
Plasmotype

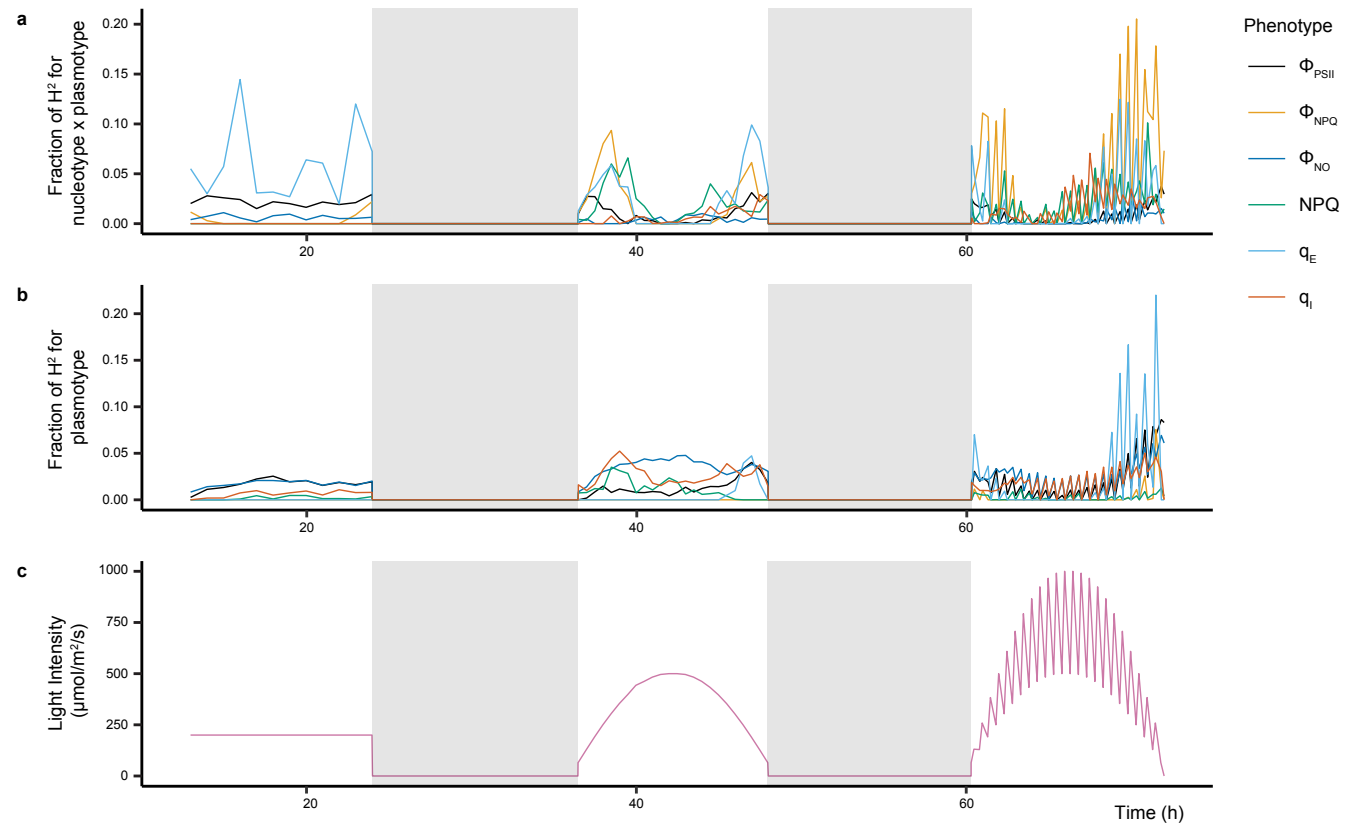
a
Fraction of H² for nucleotype x plasmotype
0.20
0.15
0.10
0.05
0.00
20
40
60
b
Fraction of H² for plasmotype
0.20
0.15
0.10
0.05
0.00
20
40
60
c
Light Intensity (µmol/m²/s)
1000
750
500
250
0
20
40
60
Time (h)
Phenotype
ΦPSII
ΦNPQ
ΦNO
NPQ
qE
qI

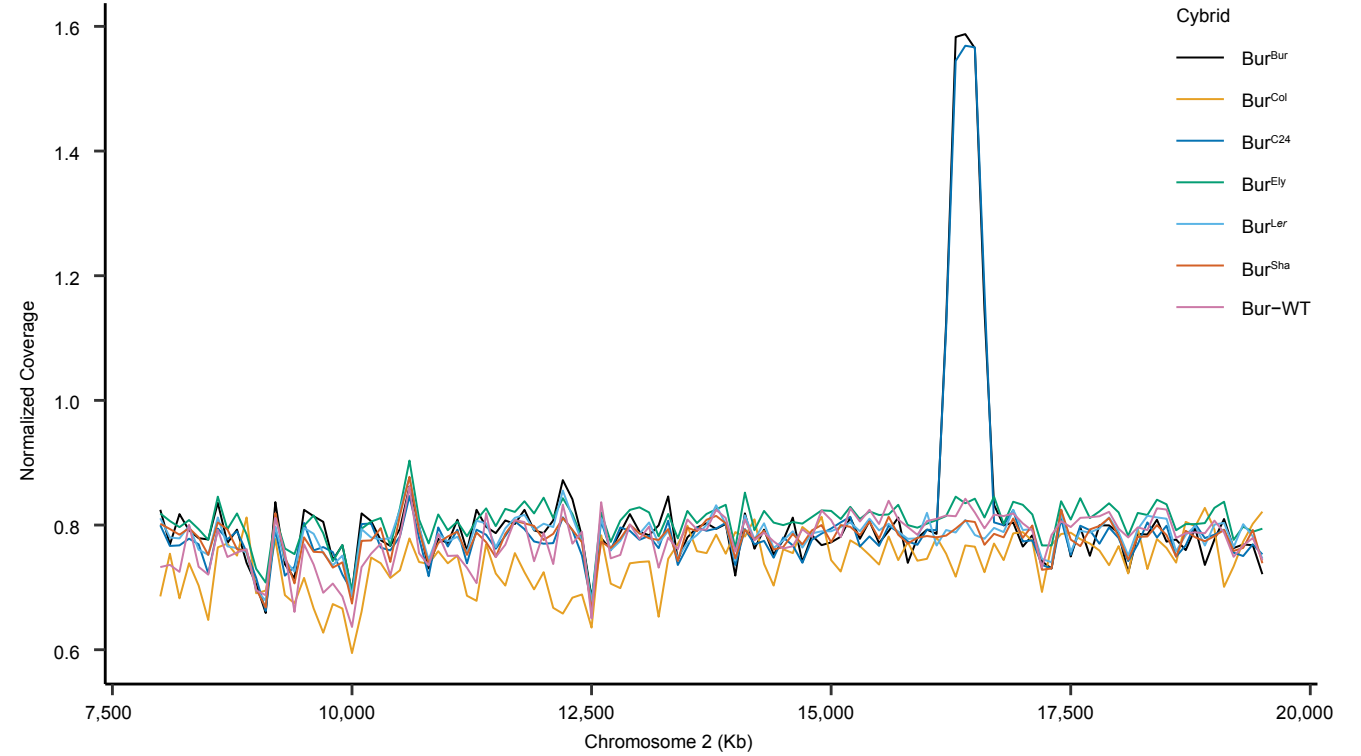
Cybrid
Bur^Bur
Bur^Col
Bur^C24
Bur^Ely
Bur^Ler
Bur^Sha
Bur−WT
Normalized Coverage
1.6
1.4
1.2
1.0
0.8
0.6
7,500
10,000
12,500
15,000
17,500
20,000
Chromosome 2 (Kb)

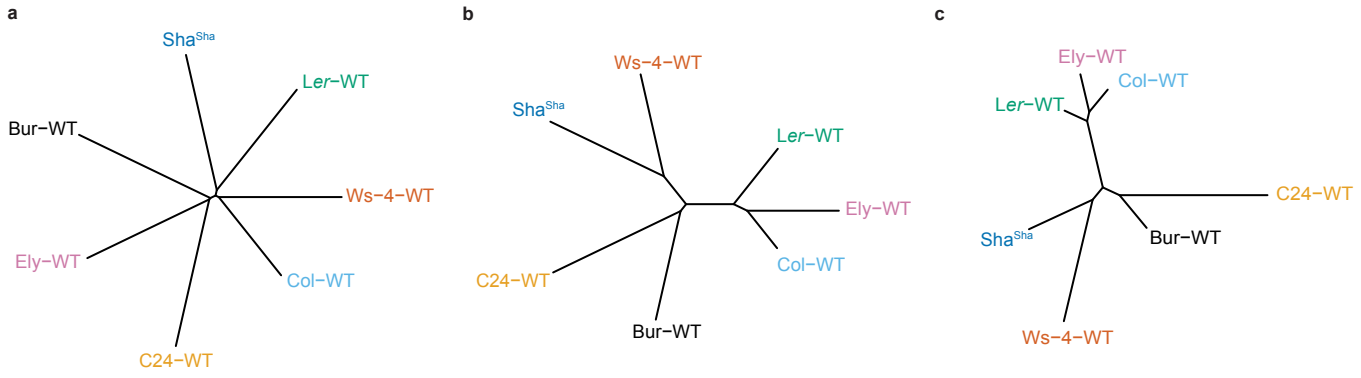
a
Sha^Sha
Ler-WT
Bur-WT
Ws-4-WT
Ely-WT
Col-WT
C24-WT
b
Ws-4-WT
Sha^Sha
Ler-WT
Ely-WT
Col-WT
C24-WT
Bur-WT
c
Ely-WT
Col-WT
Ler-WT
C24-WT
Sha^Sha
Bur-WT
Ws-4-WT

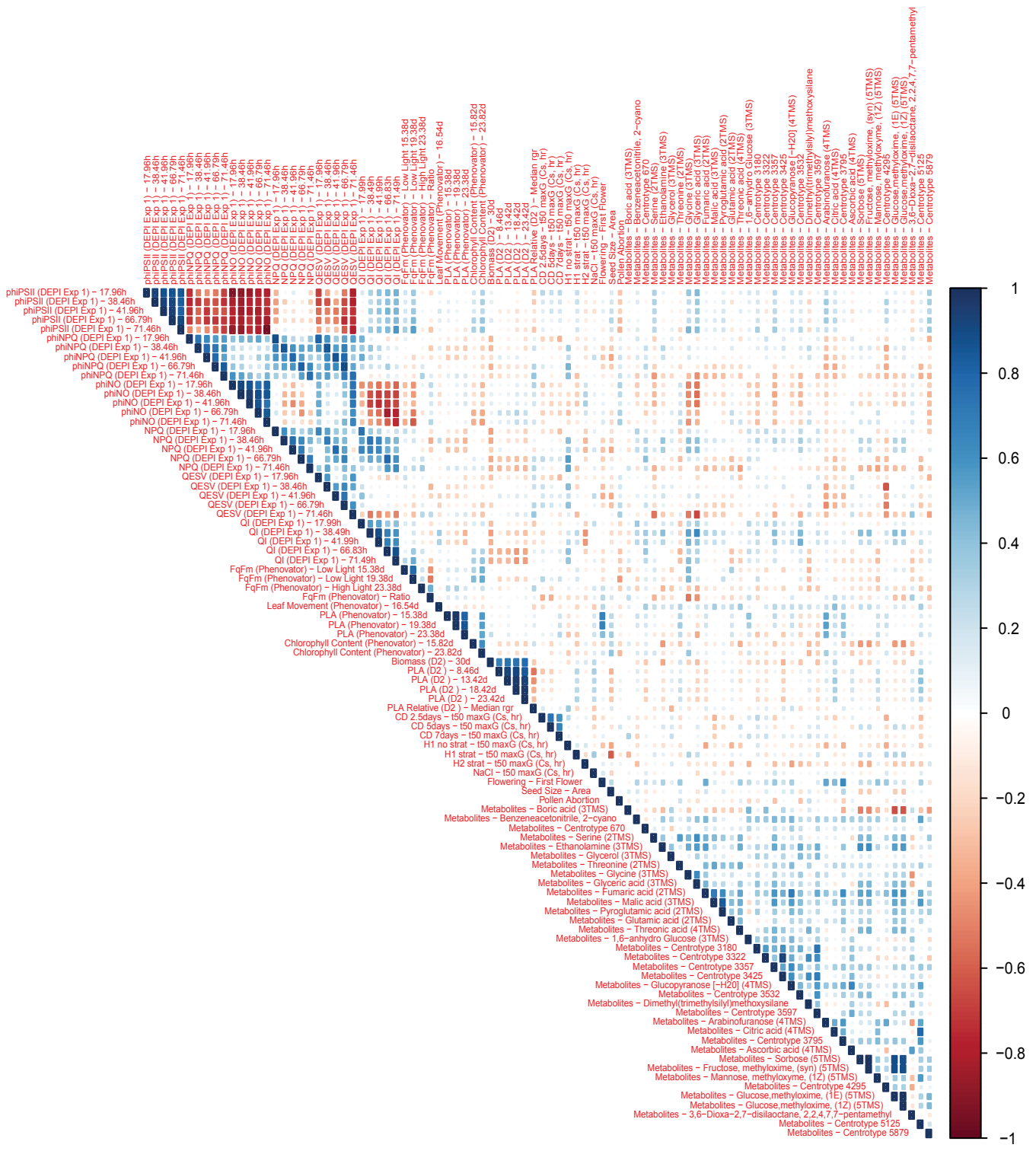
phiPSII (DEPI Exp 1) − 17.96h
phiPSII (DEPI Exp 1) − 38.46h
phiPSII (DEPI Exp 1) − 41.96h
phiPSII (DEPI Exp 1) − 66.79h
phiPSII (DEPI Exp 1) − 71.46h
phiNPQ (DEPI Exp 1) − 17.96h
phiNPQ (DEPI Exp 1) − 38.46h
phiNPQ (DEPI Exp 1) − 41.96h
phiNPQ (DEPI Exp 1) − 66.79h
phiNPQ (DEPI Exp 1) − 71.46h
phiNO (DEPI Exp 1) − 17.96h
phiNO (DEPI Exp 1) − 38.46h
phiNO (DEPI Exp 1) − 41.96h
phiNO (DEPI Exp 1) − 66.79h
phiNO (DEPI Exp 1) − 71.46h
NPQ (DEPI Exp 1) − 17.96h
NPQ (DEPI Exp 1) − 38.46h
NPQ (DEPI Exp 1) − 41.96h
NPQ (DEPI Exp 1) − 66.79h
NPQ (DEPI Exp 1) − 71.46h
QESV (DEPI Exp 1) − 17.96h
QESV (DEPI Exp 1) − 38.46h
QESV (DEPI Exp 1) − 41.96h
QESV (DEPI Exp 1) − 66.79h
QESV (DEPI Exp 1) − 71.46h
QI (DEPI Exp 1) − 17.99h
QI (DEPI Exp 1) − 38.49h
QI (DEPI Exp 1) − 41.99h
QI (DEPI Exp 1) − 66.83h
QI (DEPI Exp 1) − 71.49h
FqFm (Phenovator) − Low Light 15.38d
FqFm (Phenovator) − Low Light 19.38d
FqFm (Phenovator) − High Light 23.38d
FqFm (Phenovator) − Ratio
Leaf Movement (Phenovator) − 16.54d
PLA (Phenovator) − 15.38d
PLA (Phenovator) − 19.38d
PLA (Phenovator) − 23.38d
Chlorophyll Content (Phenovator) − 15.82d
Chlorophyll Content (Phenovator) − 23.82d
Biomass (D2) − 30d
PLA (D2) − 8.46d
PLA (D2) − 13.42d
PLA (D2) − 18.42d
PLA (D2) − 23.42d
PLA Relative (D2) − Median rgr
CD 2.5days − t50 maxG (Cs, hr)
CD 5days − t50 maxG (Cs, hr)
CD 7days − t50 maxG (Cs, hr)
H1 no strat − t50 maxG (Cs, hr)
H1 strat − t50 maxG (Cs, hr)
H2 strat − t50 maxG (Cs, hr)
NaCl − t50 maxG (Cs, hr)
Flowering − First Flower
Seed Size − Area
Pollen Abortion
Metabolites − Boric acid (3TMS)
Metabolites − Benzeneacetonitrile, 2−cyano
Metabolites − Centrotype 670
Metabolites − Serine (2TMS)
Metabolites − Ethanolamine (3TMS)
Metabolites − Glycerol (3TMS)
Metabolites − Threonine (2TMS)
Metabolites − Glycine (3TMS)
Metabolites − Glyceric acid (3TMS)
Metabolites − Fumaric acid (2TMS)
Metabolites − Malic acid (3TMS)
Metabolites − Pyroglutamic acid (2TMS)
Metabolites − Glutamic acid (2TMS)
Metabolites − Threonic acid (4TMS)
Metabolites − 1,6−anhydro Glucose (3TMS)
Metabolites − Centrotype 3180
Metabolites − Centrotype 3322
Metabolites − Centrotype 3357
Metabolites − Centrotype 3425
Metabolites − Glucopyranose [−H2O] (4TMS)
Metabolites − Centrotype 3532
Metabolites − Dimethyl(trimethylsilyl)methoxysilane
Metabolites − Centrotype 3597
Metabolites − Arabinofuranose (4TMS)
Metabolites − Citric acid (4TMS)
Metabolites − Centrotype 3795
Metabolites − Ascorbic acid (4TMS)
Metabolites − Sorbose (5TMS)
Metabolites − Fructose, methyloxime, (syn) (5TMS)
Metabolites − Mannose, methyloxyme, (1Z) (5TMS)
Metabolites − Centrotype 4295
Metabolites − Glucose,methyloxime, (1E) (5TMS)
Metabolites − Glucose,methyloxime, (1Z) (5TMS)
Metabolites − 3,6−Dioxa−2,7−disilaoctane, 2,2,4,7,7−pentamethyl
Metabolites − Centrotype 5125
Metabolites − Centrotype 5879
1
0.8
0.6
0.4
0.2
0
−0.2
−0.4
−0.6
−0.8
−1

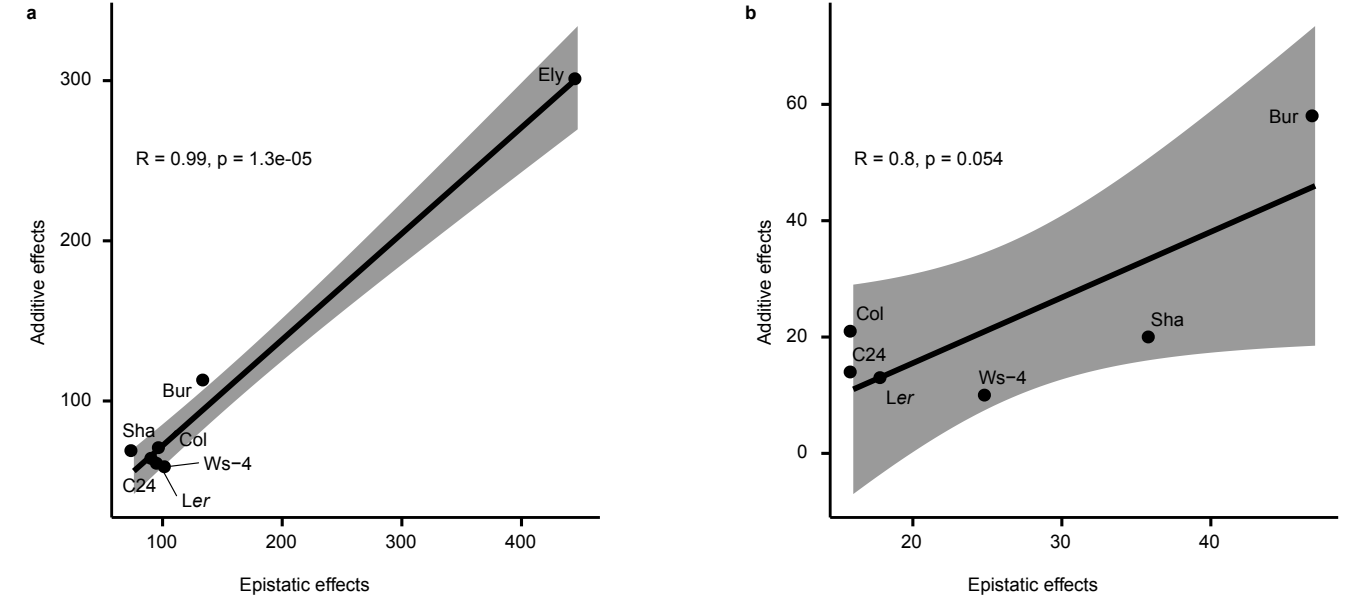
a
300
200
100
Additive effects
R = 0.99, p = 1.3e-05
Ely
Bur
Sha
Col
Ws−4
C24
Ler
100
200
300
400
Epistatic effects
b
60
40
20
0
Additive effects
R = 0.8, p = 0.054
Bur
Col
Sha
C24
Ws−4
Ler
20
30
40
Epistatic effects

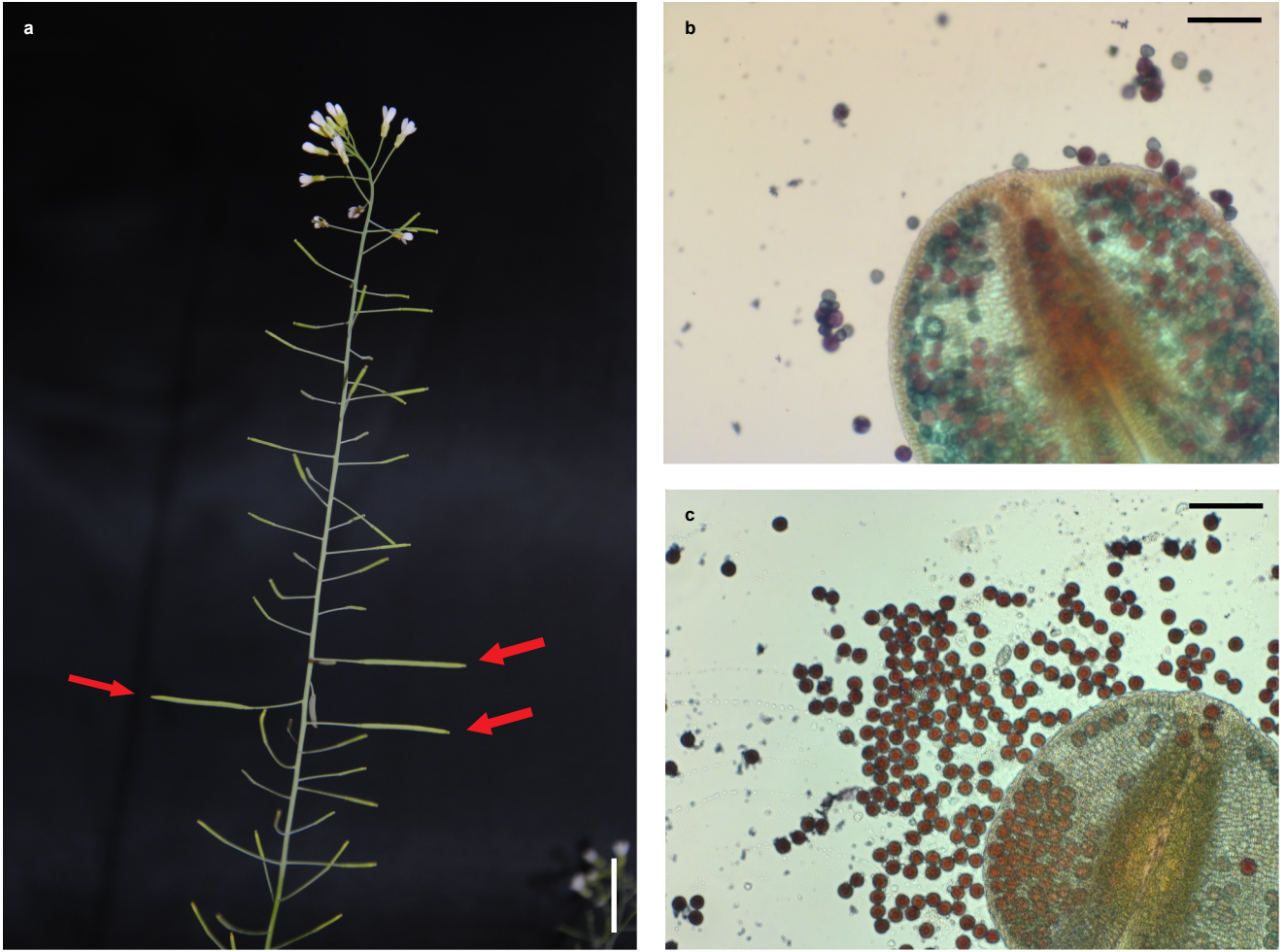
a
b
c

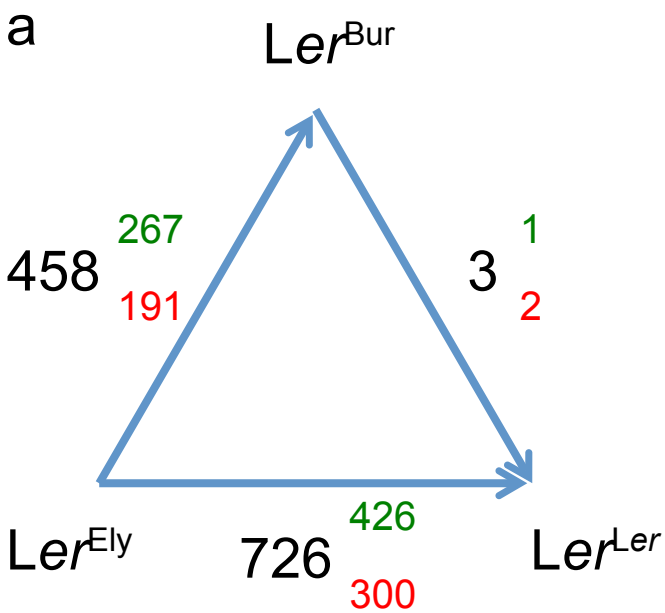
a
Ler^Bur
458
267
191
3
1
2
Ler^Ely
726
426
300
Ler^Ler

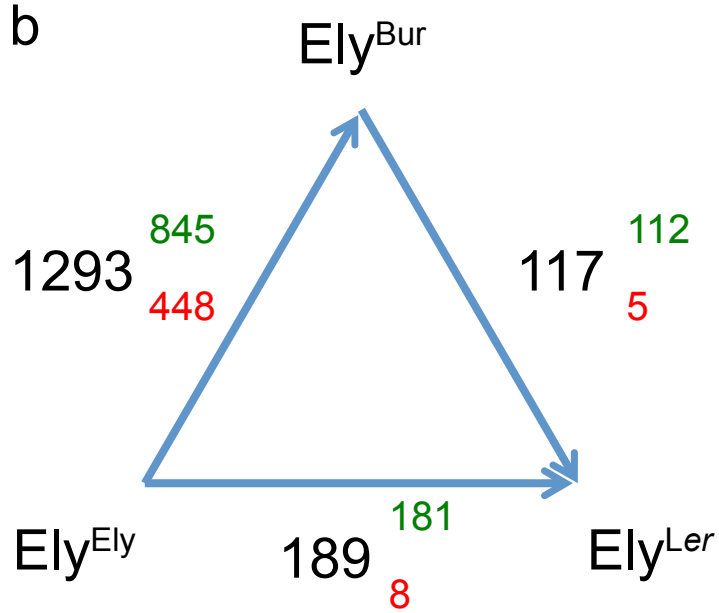
b
Ely^Bur
1293
845
448
117
112
5
Ely^Ely
189
181
8
Ely^Ler

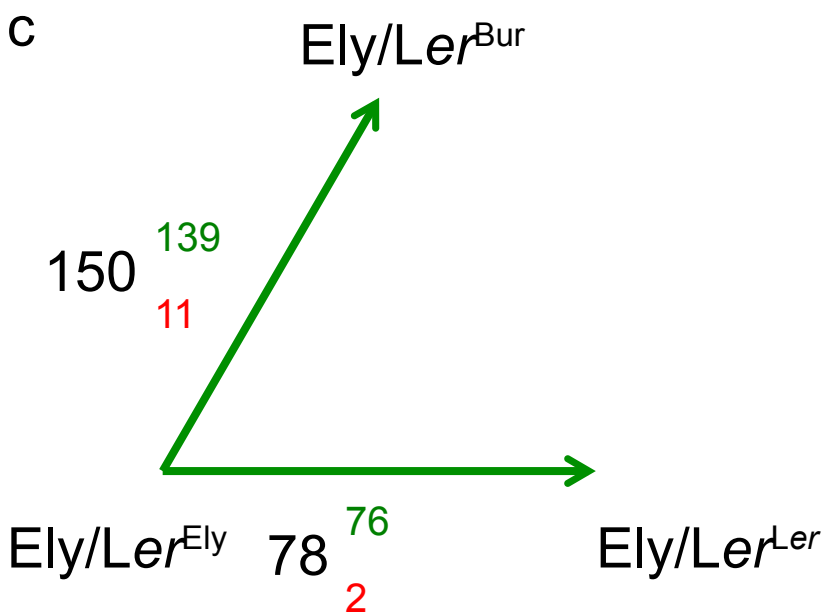
c
Ely/Ler^Bur
150
139
11
Ely/Ler^Ely
78
76
2
Ely/Ler^Ler

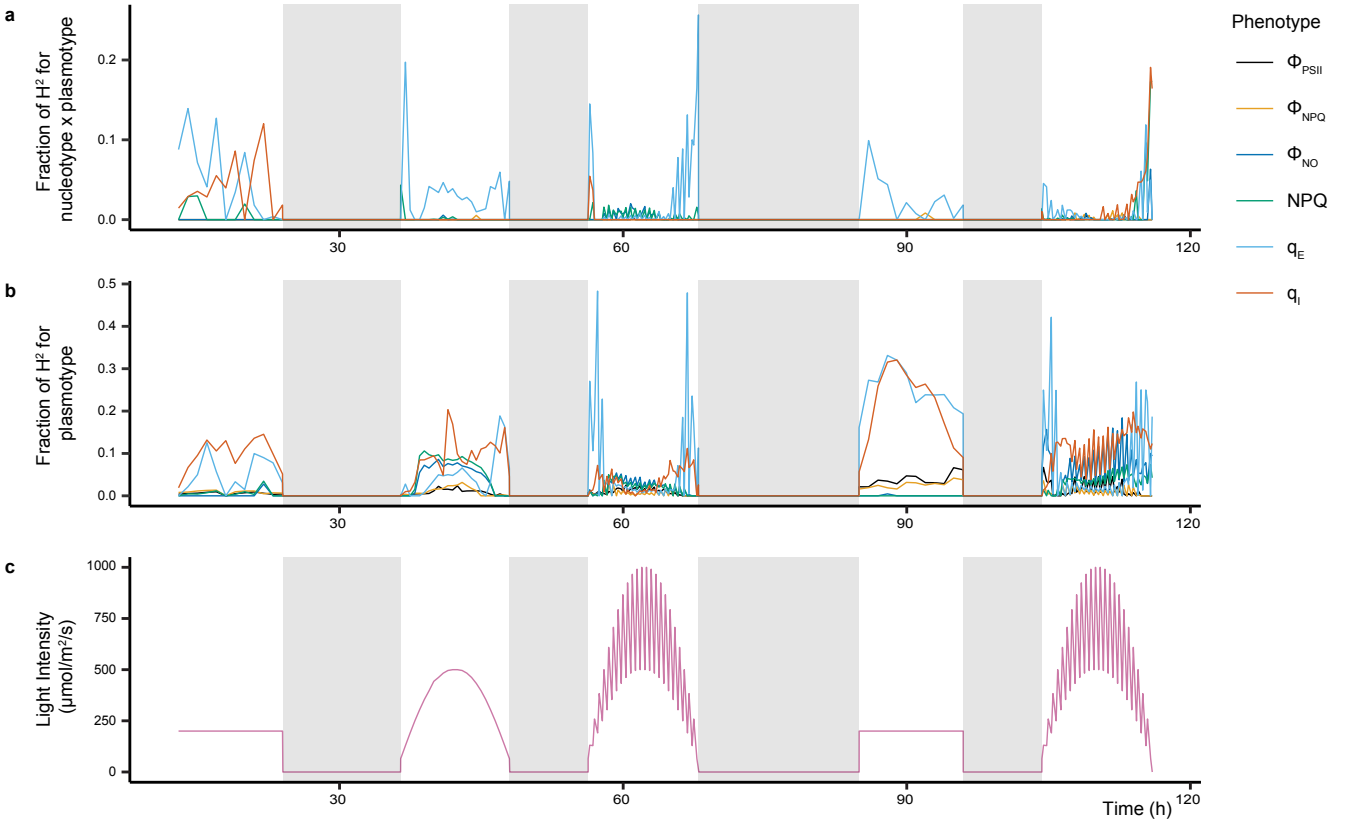
a
Fraction of H² for nucleotype x plasmotype
0.0
0.1
0.2
30
60
90
120
b
Fraction of H² for plasmotype
0.0
0.1
0.2
0.3
0.4
0.5
30
60
90
120
c
Light Intensity (µmol/m²/s)
0
250
500
750
1000
30
60
90
120
Time (h)
Phenotype
ΦPSII
ΦNPQ
ΦNO
NPQ
qE
qI

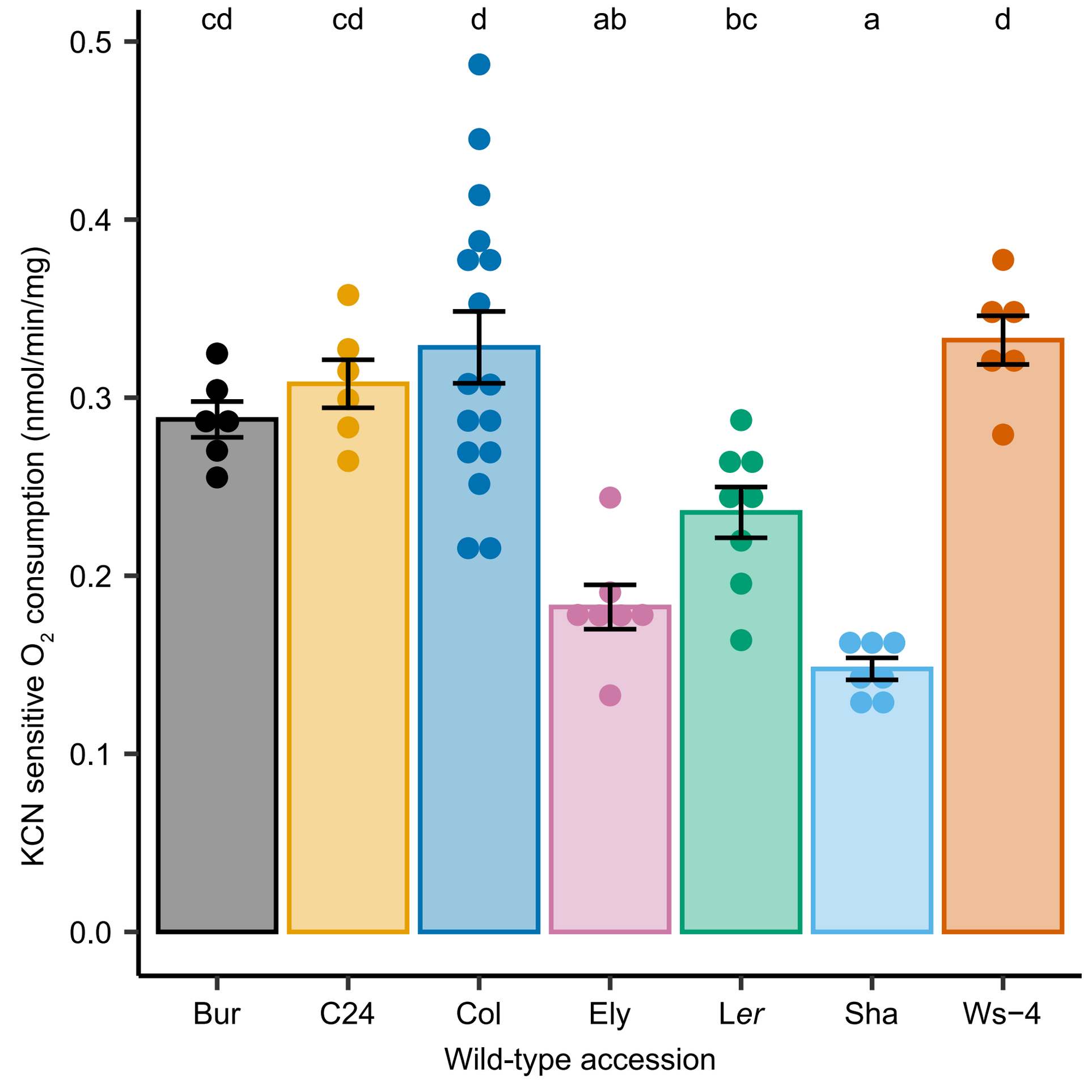
cd
cd
d
ab
bc
a
d
0.5
0.4
0.3
0.2
0.1
0.0
KCN sensitive O_2 consumption (nmol/min/mg)
Bur
C24
Col
Ely
Ler
Sha
Ws−4
Wild-type accession

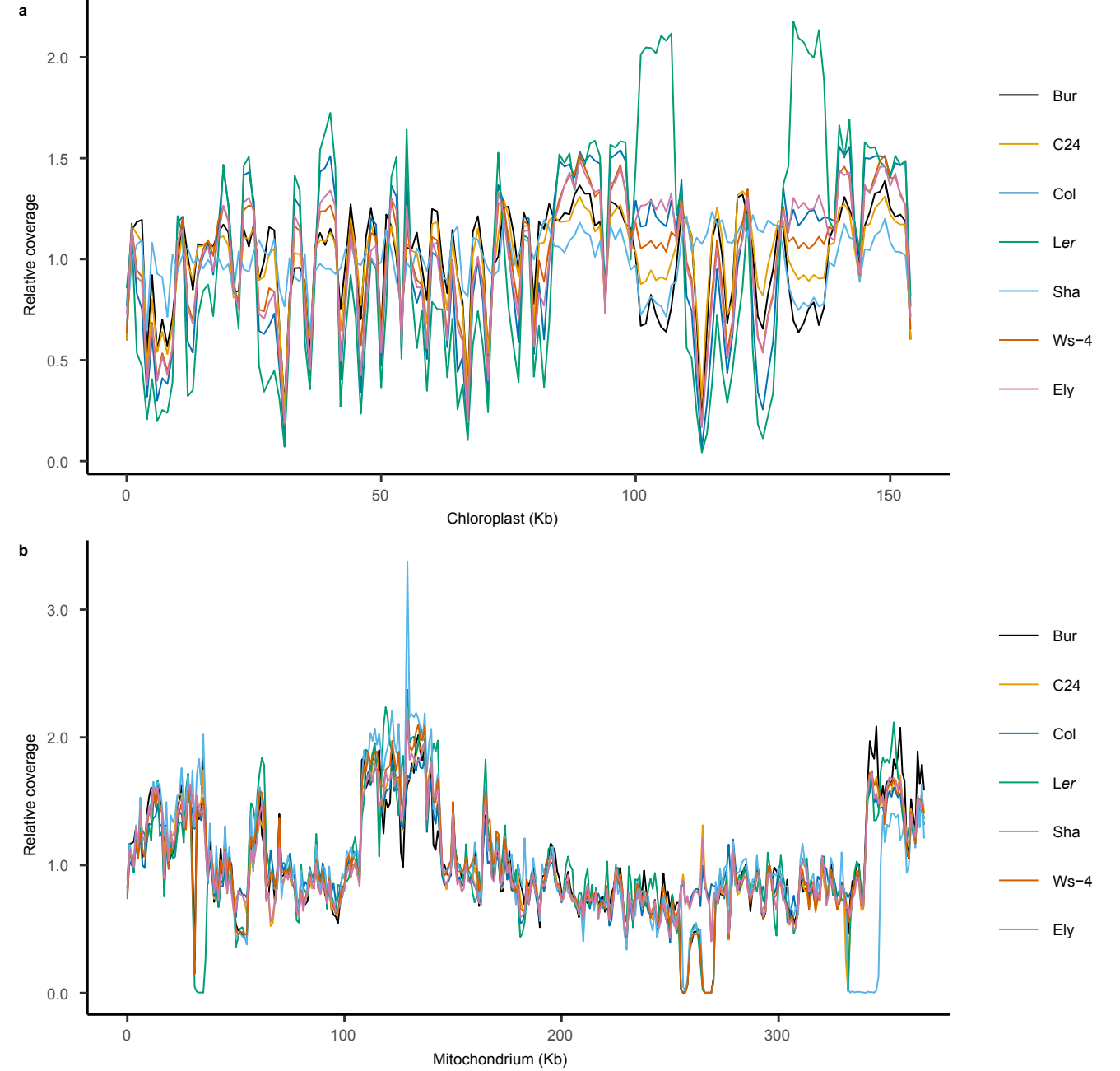
a
Relative coverage
0.0
0.5
1.0
1.5
2.0
0
50
100
150
Chloroplast (Kb)
Bur
C24
Col
Ler
Sha
Ws−4
Ely
b
Relative coverage
0.0
1.0
2.0
3.0
0
100
200
300
Mitochondrium (Kb)
Bur
C24
Col
Ler
Sha
Ws−4
Ely